ELECTROMAGNETIC
RESEARCH REPORT

LEVEL

AD A094228

SDP

DTIC
ELECTE
JAN 27 1981
S

UNIVERSITY OF KENTUCKY
ENGINEERING

Department of Electrical Engineering
University of Kentucky
Lexington, Kentucky 40506

SOME NUMERICAL METHODS FOR

EXPONENTIAL ANALYSIS WITH

CONNECTION TO A GENERAL IDENTIFICATION

SCHEME FOR LINEAR PROCESSES

Jon Richard Auton*
L. Wilson Pearson

University of Kentucky
Electromagnetics Research Report
80-5
November 1980

*Now with Effects Technology, Inc., Santa Barbara, CA.

80 12 17 006

REPORT DOCUMENTATION PAGE		READ INSTRUCTIONS BEFORE COMPLETING FORM
1. REPORT NUMBER 14 RR-80-5	2. GOVT ACCESSION NO. AD-A094 228	3. RECIPIENT'S CATALOG NUMBER
4. TITLE (and Subtitle) SOME NUMERICAL METHODS FOR EXPONENTIAL ANALYSIS WITH CONNECTION TO A GENERAL IDENTIFICATION SCHEME FOR LINEAR PROCESSES		5. TYPE OF REPORT & PERIOD COVERED Technical Report 15 May 1978 - 15 Feb 1980
		6. PERFORMING ORG. REPORT NUMBER 80-5
7. AUTHOR(s) Jon R. Auton L. Wilson Pearson		8. CONTRACT OR GRANT NUMBER(s) ONR Contract No. N00014-77-C-0362
9. PERFORMING ORGANIZATION NAME AND ADDRESS Department of Electrical Engineering University of Kentucky Lexington, KY 40506		10. PROGRAM ELEMENT, PROJECT, TASK AREA & WORK UNIT NUMBERS
11. CONTROLLING OFFICE NAME AND ADDRESS Electronics and Solid State Sciences Program (Code 427) Office of Naval Research 800 North Quincy Street, Arlington, VA 22217		12. REPORT DATE November 1980
		13. NUMBER OF PAGES 70
14. MONITORING AGENCY NAME & ADDRESS(if different from Controlling Office)		15. SECURITY CLASS. (of this report) UNCLASSIFIED
		15a. DECLASSIFICATION/DOWNGRADING SCHEDULE

16. DISTRIBUTION STATEMENT (of this Report)

DISTRIBUTION STATEMENT A

Approved for public release;
Distribution Unlimited

17. DISTRIBUTION STATEMENT (of the abstract entered in Block 20, if different from Report)

18. SUPPLEMENTARY NOTES

19. KEY WORDS (Continue on reverse side if necessary and identify by block number)

system identification, Prony, exponential analysis,
Singularity Expansion Method, transient

20. ABSTRACT (Continue on reverse side if necessary and identify by block number) A general identification scheme for linear processes is presented and related to some well-known exponential analysis methods such as Prony's method and the pencil-of-functions method. An elucidating explanation of the source of error (bias) for the general scheme is given. Some variations of the pencil-of-functions method are given an intense examination with some revealing numerical examples. A new exponential analysis method, called the adaptive method, is developed from the general scheme. Numerical examples of the adaptive method demonstrate its excellent performance in the presence at high levels of noise. Recommendations are made concerning the use of the adaptive method and directions for further work.

DD FORM 1473 EDITION OF 1 NOV 65 IS OBSOLETE
1 JAN 73

ACKNOWLEDGEMENTS

iii

TABLE OF CONTENTS

LIST OF TABLES

LIST OF FIGURES

CHAPTER I

INTRODUCTION

1.1 Exponential Analysis as a Special Case

of Systems Identification

Exponential analysis attempts to characterize a waveform with a
sum of complex exponentials, that is, a sum of damped sinusoidal com-
ponents. Consider the class of linear processes whose impulse re-
sponses are representable as a sum of exponential components. If the
impulse response, possibly noise contamined, is given for a process in
this class, the transfer function of that process can be estimated by
applying a body of theory known as systems identification [1,2,3,4].
The impulse response can be expressed as the inverse transform (either
the inverse Laplace transform or the inverse z-transform) of the
partial-fraction expansion of this estimated transfer function. If
the waveform to be analyzed is assumed to be the impulse response
of a process of this class, then the systems identification technique
plus the process of partial-fraction expansion can be viewed as an
exponential analysis method. Hence, exponential analysis methods can
be equated to systems identification methods for the case of impulse
input to the process. The poles of the transfer function are the
damped resonances that characterize the waveform. The imaginary
parts of the poles are the angular frequencies of the sinusoidal com-
ponents and the real parts are the corresponding damping constants.

1.2 Motivation for Exponential Analysis and

a Survey of the Literature

Systems identification theory and exponential analysis find appli-
cations in such diverse fields as industrial controls, econcmic model-
ing and in the analysis of biological systems. Recently, these iden-
tification methods have found application in the extraction of the
singularity expansion method (SEM) description of a cransient scatterer
from its time domain response as was first suggested by Mittra and Van
Blaricum [5]. SEM was developed by Baum [6, 7] from the insight that
the transient response of a scatterer resembles a sum of exponentially
damped sinusoids.   The least-squares Prony's method was proposed by
Van Blaricum and Mittra [8, 9] as a means of obtaining the SEM descrip-
tion from the transient response of a scatterer. Pearson and Roberson
[10] have since developed and documented a method of obtaining the com-
plete SEM description of a scatterer from   transient response data.
Dudley [11] related Prony's method to a parametric system model and
proceeded to demonstrate a bias in the estimates of the system poles
inherent in least-squares Prony's method.

The parametric model employed by Dudley is a modified version of
the generalized model described by Eykhoff [1, 2], Astrom and Eykhoff
[3], and on pages 209-220 of Eykhoff [4]. The origin of the general-
ized model can be traced to Kalman in 1958 [12] who assumes noise-free
input and output records of the process to be identified. This is the
assumption from which the generalized model derives its validity. With
noise, this model is no longer valid, and the resulting transfer func-
tion estimate is slightly erroneous.

Steiglitz and McBride [13] introduced a so-called actual model that differs from the Kalman or generalized model by using the model output in place of the noise corrupted process output for the feedback inherent in the model. The validity of the actual model does not break down when noise is present in the process output. However, the estimation of the parameters of the actual model is a highly nonlinear problem. One major reason for the generalized model's popularity is linearity in the parameters allowing one-shot estimation. In contrast, an iterative estimation procedure is required by the actual model.

Another related method is the pencil-of-functions method advocated by Sarkar [14, 15]. The method was originally proposed by Jain and Gupta [16] and elaborated on by Jain [17, 18, 19]. In [15] Sarkar indicates connections between Prony's method, the Wiener filter, and the pencil-of-functions method.

One important property of the actual model is that when it is used for exponential analysis, it produces a "best fit" to the waveform under analysis in the mean-square sense, that is, it minimizes the mean-square error. Some other methods that have this property are found in references [13,20,21,22,23].

1.3 The Contribution of the Present Work

The original intent of this work was to develop a noise tolerant, efficient method for exponential analysis. The method was to find direct application in extraction of the SEM description of a scatterer from measured surface currents. A new noise tolerant method is presented in this document. Unfortunately, the method is laborious, and hence, only partial success can be claimed with regard to the original intent.

Perhaps the real contribution of the present work is the conceptual groundwork which is a prerequisite for further improvements on exponential analysis methods. This groundwork is laid by defining a general scheme that incorporates most, if not all, exponential analysis methods and by defining the sources of difficulties for such methods. This groundwork is established through a new formulation of an extended generalized model and an extended actual model after Steiglitz and McBride [13]. The extension is to admit any set of linear filter functions to form generalized filter sections in the respective models. Emphasis is placed on concept development rather than strict mathematical rigor which would stifle such development.

In Chapter II one major source of difficulty with exponential analysis methods is defined. This difficulty is the parameter bias that Dudley [11] brought to light. An attempt is made to relate the source of this so-called bias to the distinction made by Steiglitz and McBride [13] between the true error model and the linear regression model. Also presented in Chapter II is the general identification scheme that is used through the rest of this work.

Chapter III relates Prony's method and the pencil-of-functions method to the general scheme of Chapter II. The various problems associated with the pencil-of-functions method are discussed, and simple remedies to those problems are proposed.

Chapter IV introduces a new method, called the adaptive method, which is highly tolerant of the presence of noise in the waveform under analysis.

Chapter V presents conclusions and indicates directions in which future research may be fruitful.

1.4 Notational Conventions

The following conventions of notation are observed:

1. The symbol "s" denotes the Laplace-transform variable. If the transfer function of a process is a function of s, the process is assumed to be a continuous-time process.

2. The symbol "z" denotes the z-transform variable. If the transfer function of a process is a function of z, the process is assumed to be a discrete-time, sampled-data process.

3. If a symbol for a transfer function appears alone, without the appropriate variable enclosed in parenthesis, the symbol denotes a "generalized" transfer function whose functional dependence is not restricted in any way. To illustrate, a process can be given a continuous-time representation in which case the transfer function could be a function of s, or the process can be given a discrete-time representation, then the transfer function is a function of z. If only the essence of the process is to be conveyed, without regard to its particular representation, then the transfer function is written without indicating its functional dependence.

4. An asterisk indicates the complex conjugate of the expression preceding it.

5. The symbol "T" raised above the expression it follows indicates the transpose of the matrix or vector preceding it.

6. A prime indicates the transpose conjugate of the matrix or vector preceding it.

Other symbols used in this work are defined when they are introduced in the text.

CHAPTER II

ESTIMATION OF THE PROCESS TRANSFER FUNCTION

2.1 Introduction

The problem under consideration is the characterization of a sampled, noise contaminated waveform, $y(k)$, as a weighted sum of complex exponentials of the form

$$y_m(k) = \sum_{j=1}^{n} A_j z_j^k, \quad k = 0, \ldots, M-1 \quad (1)$$

where $z_j = \exp(s_j T)$ and T is the time duration between successive samples. The objective is to choose the A_j and z_j that best characterize the waveform. Usually the best characterization is assumed to be the one that minimizes the mean-squared error between the waveform and the characterization.

It is assumed that $y(k)$ is the noise contaminated, impulse response of the linear process with a nth order transfer function given by

$$H = \frac{b_1 F_1 + \cdots + b_n F_n}{a_o + a_1 F_1 + \cdots + a_n F_n} \quad . \quad (2)$$

The F_i are predefined functions of the transform variable. For example, the F_i could be polynomials in the transform variable. Later the F_i are related to filtering operations, and for this reason, they are referred to as "filter transfer functions." With appropriate choices of the a_i, b_i, and F_i, any transfer function can be represented in this form. The reason this form is used is because the general parametric model introduced in the next section also has a transfer function of this form. The F_i are the transfer functions (which are not specified explicitly in order to remain completely general) of the filters that make up the model.

The problem can be restated as the estimation of (2). By expanding the estimated transfer function in partial fractions and performing an inverse transform, the desired characterization is obtained. The z_i or s_i can be interpreted as the poles of (2) and the A_i are the corresponding residues of (2). The z_i and s_i are related by $z_i = \exp(s_i T)$.

2.2 Two Parametric Models

Steiglitz and McBride describe two parametric models in terms of which they interpret their identification procedure. A straightforward extension of these parametric models provides a framework that is broader in its applicability. They are specialized herein to describe the Prony procedure [24], the so-called least squares Prony procedure [9], and the pencil-of-functions method of Jain [19]. The models are used further to provide a new iterative identification procedure that appears to be substantially more tolerant to noise-corruption in data than existing schemes. The first, the actual or true model, is shown in Figure 1 and has the transfer function

$$H_m = \frac{\beta_1 F_1 + \cdots + \beta_n F_n}{\alpha_o + \alpha_1 F_1 + \cdots + \alpha_n F_n} \ . \tag{3}$$

The second model is called the approximate model and is shown in Figure 2. The approximate model is derived from the actual model by approximating the model output with the noisy process output as the source of feedback in the model. It should be noted that (3) is not the transfer function of the approximate model. In fact, a transfer function that serves as a useful approximation to the process transfer function cannot be defined for the approximate model. These models reduce to those of [13] if the F_j's are chosen in the form of rational polynomials in the z-transform variable that have a zero at $z = 0$.
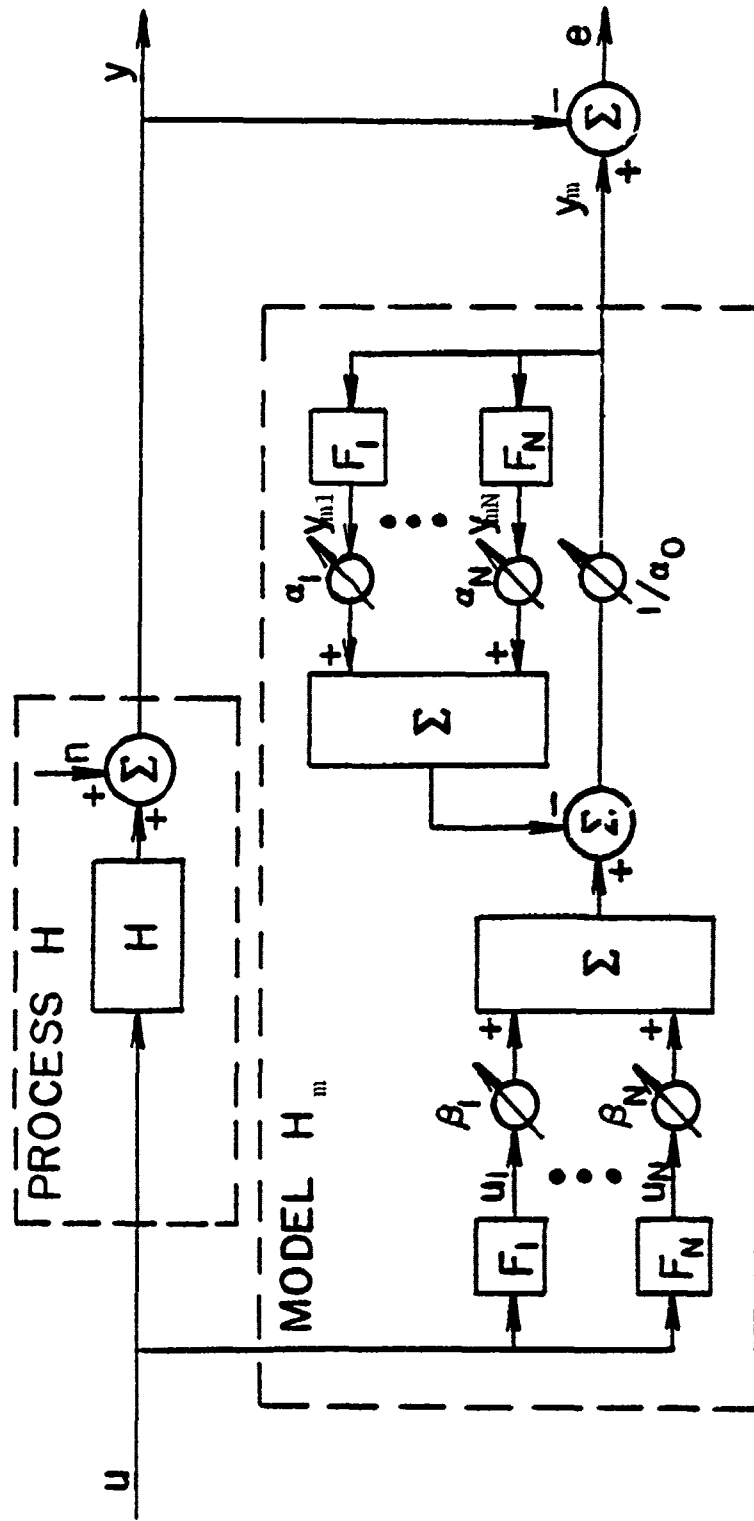
Figure 1. The actual model is shown in the dashed box labeled "model." The parameters, α_i and β_i, scale the output, y_{mi} and u_i, of filters, F_i. The scaled outputs are summed to form the model output, y_m, which is compared with the process output, y, to form the error, e. The identification Procedure chooses the model parameter values that minimize the error.
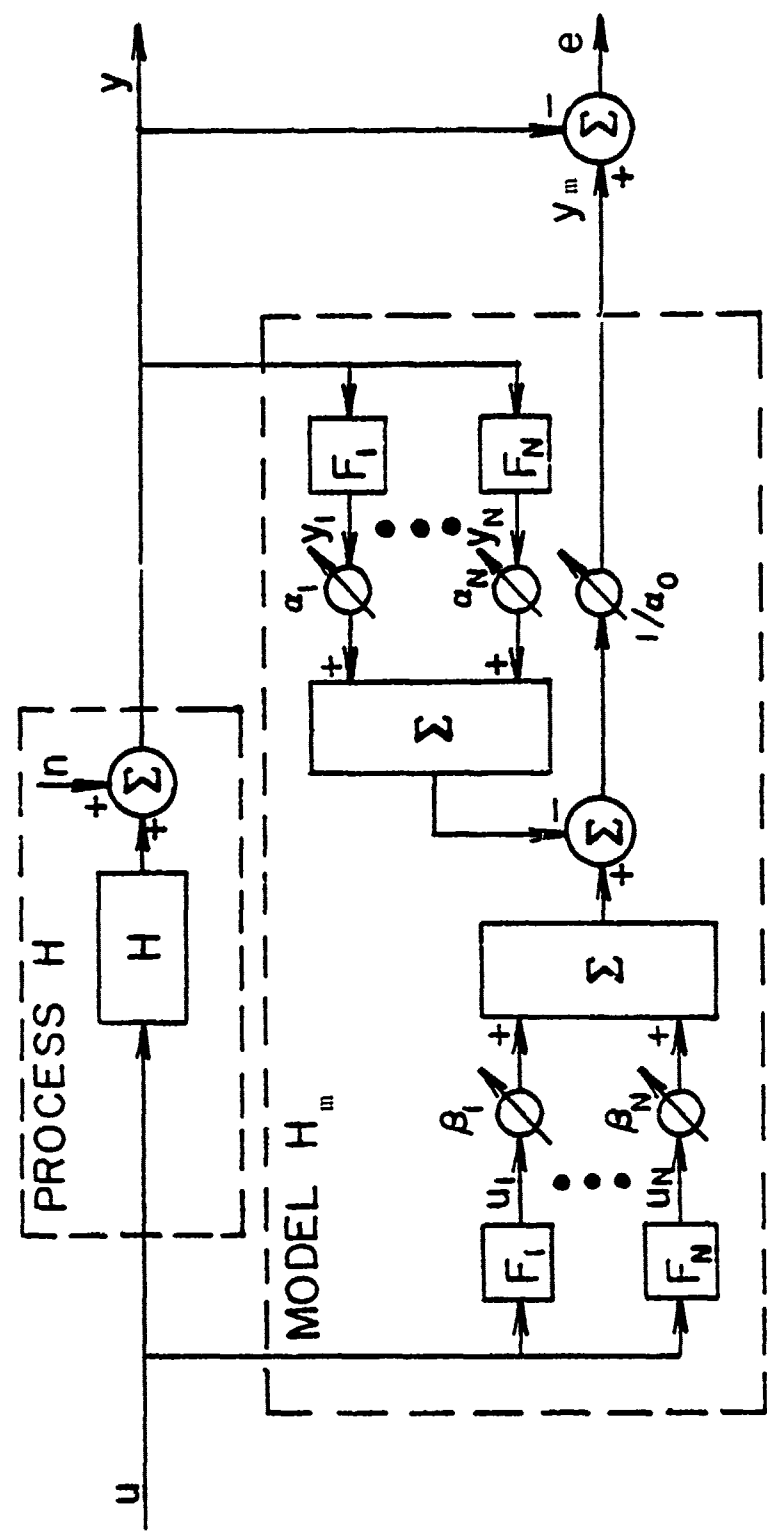
Figure 2. The approximate model is shown in the dashed box labeled "model." The parameters, α_i and β_i, scale the outputs, y_i and u_i, of filters, F_i. The scaled outputs are summed to form the model output, y_m, which is compared with the process output, y, to form the error, e. The identification procedure chooses the model parameter values that minimize the error.

The object of the identification process is to adjust the parameters of the model to minimize the mean-squared error, $E = ||e||^2$. An estimate of the process transfer function is found by using those minimizing parameters along with filter transfer functions, F_i, in (3). Routinely, the parameters that minimize the error norm in the approximate model are used in (3) even though it is the transfer function of a different model. The result is an estimate of the process transfer function whose error depends upon the strength of the noise process "n".

Why bother with the approximate model if better estimates can be had using the actual model? This question is quickly answered when one attempts to estimate the parameters of the actual model. Because the model output and the parameters are interdependent, the parameter estimation problem is highly nonlinear, and must be solved by iterative methods. In the approximate model, the parameter-invariant process output replaces the model output, thereby making the problem linear. Hence, the approximate model is widely preferred.

2.3 Estimation of the Model Parameters

An estimator is a rule for choosing the model parameter values in a way that tends to minimize the error between the process output and the model output. Two types of estimators are distinguished: discrete-time and continuous-time.

The discrete estimator operates on sampled data and produces an estimate of the pulse transfer function of the process. The discrete mean-square error is defined as $E = \underline{e}'\underline{e}$ where $\underline{e} = [e(0) \ldots e(M-1)]^T$ is a column vector consisting of the sampled sequence.

Likewise, the model output sequence and filter output sequences

are denoted as M-length vectors $\underline{y}_m$ and $\underline{y}_i$, $\underline{u}_i$ for $i=1,\ldots,n$, respectively. The output of the approximate model can be expressed as

$$\underline{y}_m = \sum_{i=1}^{n} \frac{-\alpha_i \ \underline{y}_i + \beta_i \underline{u}_i}{\alpha_o} = \frac{\Omega \ \underline{\theta}}{\alpha_o}$$

where

$$\Omega \equiv \begin{bmatrix} y_1(0) \ \ldots \ y_n(0) & u_1(0) \ \ldots \ u_n(0) \\ \vdots & \vdots & \vdots & \vdots \\ y_1(M-1) \ \ldots \ y_n(M-1) & u_1(M-1) \ldots \ u_n(M-1) \end{bmatrix},$$

and $\underline{\theta}$ is the vector of model parameters

$$\underline{\theta} \equiv [-\alpha_1 \ldots \ -\alpha_n \beta_1 \ldots \beta_n]^T.$$

The process output is denoted by an M-length vector $\underline{y}$. The error can then be written as

$$\underline{e} = \frac{\Omega \ \underline{\theta}}{\alpha_o} - \underline{y} \ .$$

It can be shown that the partial derivatives of E with respect to the real parts of the parameters are

$$\frac{\partial E}{\partial \text{Re}\alpha_j} = 2 \ \text{Re}[\frac{-\underline{e}'\underline{y}_j}{\alpha_o}],$$

and

$$\frac{\partial E}{\partial \text{Re}\beta_j} = 2 \ \text{Re}[\frac{\underline{e}'\underline{u}_j}{\alpha_o}],$$

for $j=1,\ldots,n$. A necessary condition that a set of parameters must satisfy in order to minimize E is that the partial derivatives listed above vanish. This leads to the set of normal equations

$$\underline{e}'\underline{y}_j = 0,$$

$$\underline{e}'\underline{u}_j = 0,$$

for j=1,..., n which can be written in matrix form as

$$\Omega' \underline{e} = 0$$

or $\qquad \Omega' [\frac{\Omega \theta}{\alpha_o} - \underline{y}] = 0$.

Solving this equation for $\underline{\theta}$ produces the <u>discrete least-squares</u> <u>estimator</u>:

$$\underline{\theta} = [\Omega'\Omega]^{-1} \Omega' \alpha_o \underline{y} \quad . \tag{4}$$

The columns of Ω consist of the sampled filter outputs of the approximate model indicated in Figure 2. The filter output sequences can be computed with a set of difference equations that characterize the discrete filters, F_i.

If M=2n, (4) reduces to

$$\underline{\theta} = \Omega^{-1} \alpha_o \underline{y} \quad . \tag{5}$$

If M<2n, $\Omega'\Omega$ is singular because insufficient data are available to estimate 2n parameters.

The continuous estimator operates on continuous data. The filters within the model are continuous in this case. The continuous mean-square error is defined as

$$E = \langle e, e \rangle = \int_{t_1}^{t_2} e^*(t) \ e(t) dt$$

where t_1 and t_2 define the interval on which the waveform exists. The <u>continuous least-square estimator</u> has the form:

$$\underline{\theta} = G_{2n}^{-1} \alpha_o \underline{r} \tag{6a}$$

where

$$\underline{\theta} \equiv [-\alpha_1 \ \dots \ -\alpha_n \ \ \beta_1 \ \dots \ \beta_n]^T, \tag{6b}$$

$$\underline{r} = [\langle y, \dot{y}_1 \rangle \quad \cdots \quad \langle y, \dot{y}_n \rangle \langle y, u_1 \rangle \quad \cdots \quad \langle y, u_n \rangle]^T , \quad (6c)$$

$$\text{and } G_{2n} \equiv \begin{bmatrix} \langle \dot{y}_1, \dot{y}_1 \rangle \cdots \langle \dot{y}_n, \dot{y}_1 \rangle \langle u_1, \dot{y}_1 \rangle \cdots \langle u_n, \dot{y}_1 \rangle \\ \vdots \\ \langle \dot{y}_1, \dot{y}_n \rangle \qquad \cdots \qquad \qquad \vdots \\ \langle \dot{y}_1, u_1 \rangle \qquad \cdots \qquad \qquad \vdots \\ \vdots \\ \langle \dot{y}_1, u_n \rangle \qquad \cdots \qquad \langle u_n, u_n \rangle \end{bmatrix} . \quad (6d)$$

The inner product is defined as

$$\langle x_1, x_2 \rangle = \int_{t_1}^{t_2} x_1^*(t) \; x_2(t) \; dt . \quad (6e)$$

The continuous estimator results from the minimization of the error in much the same way the discrete estimator does, and therefore, the deriviation for the continuous estimator will not be presented.

The parameters of the actual model can be estimated by an iterative procedure using a modification of the estimators described above. This procedure involves replacing the process output with the model output as the feedback source within the model. Specifically, if y_{mi}^{L-1} replaces y_i, α_i^L replaces α_i, and β_i^L replaces β_i in (4) and (6), for $i = 1,\ldots, n$, a technique of iterative improvement results. The parameters of the Lth iteration, α_i^L and β_i^L, are estimated in terms of the most recent model output, y_m^{L-1}. An initial estimate of the process is required to start this procedure. The approximate model can be used to provide this estimate. Nothing is known about the convergence characteristics of this procedure. However, Steiglitz and McBride [13]

do mention that, in general, this procedure fails to converge if the initial parameters are far from the optimum values.

CHAPTER III

EXISTING METHODS

3.1 Introduction

By necessity the models described in the previous chapter are quite general since they must serve as a common ground for the two existing methods that are examined in this chapter. Prony's method and the pencil-of-functions method are shown to be special cases of the estimation method for the approximate model. Each method corresponds to a particular choice of filters within the model.

3.2 Prony's Method

In 1795 a method for exponential analysis was invented by R. Prony [24]. The method was implemented by hand calculations. Prony's method has since found numerous applications and has sometimes been published without reference to its inventor. Van Blaricum [25] has compiled a large though abridged bibliography of Prony's method. Van Blaricum and Mittra [8,9] conducted a well documented investigation of Prony's method and proposed some useful extensions of the technique. Lager, et al. [26] have suggested a "sliding-window Prony" procedure as a means of reducing the noise sensitivity of the method.

Although Prony's method is computationally efficient, Dudley [11] demonstrated that the least-squares version [9] can produce biased pole values that differ significantly from the "best" pole values unless the noise component of the waveform is small. The "best" pole values are those that best fit the waveform. Prony's method results from the approximate model. It follows that the bias is nothing more than the slight error that is incurred by the use of the approximate model.

Prony's method results from the approximate model under the following assumptions:

1. $\alpha_n = 1$.

2. $F_i = F_i(z) = z^i$.

3. The model input is an impulse at $k = 0$.

4. $M = 2n$.

The assumption of $\alpha_n = 1$ implies that the parameters are normalized relative to α_n which is a distinguishing characteristic of Prony's method. The other methods examined in this work are normalized relative to α_0, that is, $\alpha_0 = 1$ is assumed. Since $M = 2n$, (5) may be used to estimate the parameters. In this case,

$$\underline{\theta} \equiv [-\alpha_1 \cdots -\alpha_{n-1} -1 \; \beta_1 \cdots \beta_n]^T ,$$

$$\underline{y} \equiv [y(0) \cdots y(2n-1)]^T,$$

$$\text{and } \Omega \equiv \begin{bmatrix} \begin{array}{ccc} y(1) & \cdots & y(n) \\ \cdot & & \cdot \\ \cdot & & \cdot \\ \cdot & & \cdot \\ \underline{y(n)} & \underline{\cdots} & \underline{y(2n-1)} \\ y(n+1) & \cdots & y(2n) \\ \cdot & & \cdot \\ \cdot & & \cdot \\ \cdot & & \cdot \\ y(2n) & \cdots & y(3n-1) \end{array} & \begin{array}{c} \\ \\ 0 \\ \\ \\ \\ \\ 0 \\ \\ \end{array} \end{bmatrix} .$$

The rank of Ω is, at most, n. Hence, with some rearranging the following equation results:

$$\begin{bmatrix} y(0) & \ldots & y(n-1) \\ \cdot & & \cdot \\ \cdot & & \cdot \\ \cdot & & \cdot \\ y(n-1) & \ldots & y(2n-2) \end{bmatrix} \begin{bmatrix} \alpha_0 \\ \cdot \\ \cdot \\ \cdot \\ \alpha_{n-1} \end{bmatrix} = - \begin{bmatrix} y(n) \\ \cdot \\ \cdot \\ \cdot \\ y(2n-1) \end{bmatrix} . \tag{7}$$

System (7) is equivalent to Prony's method for estimating the poles of a waveform. The poles of the process may be determined from the α_i. The β_i must be determined by other means. See, for instance, reference [11]. A straightforward way of determining the A_i of (1) is to use the poles to form exponential basis functions which are used in linear combination to form a least-squares fit to the data. The A_i are the coefficients of this linear combination. The A_i may also be found from the α_i and β_i, once these parameters are known, as simply the residues of H_m.

Examples of the performance of Prony's method under a variety of conditions are found in sufficient detail elsewhere [8, 11] and, for this reason, will not be given here.

3.3 The Pencil-of-Functions Method

The pencil-of-functions method was originally proposed by Jain and Gupta [16] before Prony's Method became well known. In this section the pencil-of-functions method is derived as a special case of the approximate model presented in Chapter II in contrast to its usual derivation from the so-called pencil-of-functions concept [19]. Additional material on the pencil-of-functions method is contained in references [14, 15, 17]. A discrete version of the method is described in reference [13].

The pencil-of-functions method results from the approximate model under the following assumptions:

1. $\alpha_o = 1$.

2. $F_i = F_i(s) = (1/s)^i$.

3. The matrix G_{2n+1}, defined in what follows, is singular.

Note that the approximate model reduces to the generalized model [1,3,

4] under the first assumption; thus, it follows that the pencil of-functions method may be derived from the generalized model. The estimator embodied in equation (6) may be used to estimate the transfer function of the process, and the poles of the process may be estimated as the zeros of the denominator of (3), viz.,

$$1 + \alpha_1 \left(\frac{1}{s}\right) + \cdots + \alpha_n \left(\frac{1}{s}\right)^n = 0$$

or

$$1s^n + \alpha_1 s^{n-1} + \cdots + \alpha_n = 0 . \tag{8}$$

The α_i may be found using the estimator of (6). By applying Cramer's rule to system (6), it can be shown that

$$\alpha_i = \Delta_{0i}/\Delta_{00} \tag{9}$$

where Δ_{pq} denotes the cofactor formed by deleting row $p+1$ and column $q+1$ of the matrix,

$$G_{2n+1} = \begin{bmatrix} \langle y,y \rangle & \langle y,y_1 \rangle & \cdots & \langle y,y_n \rangle & \langle y,u_1 \rangle & \cdots & \langle y,u_n \rangle \\ \langle y_1,y \rangle & & & & & & \\ \vdots & & & & & & \\ \langle y_n,y \rangle & & \vdots & \vdots & & & \vdots \\ \langle u_1,y \rangle & & & & & & \\ \vdots & & & & & & \\ \langle u_n,y \rangle & & \cdots & & & & \langle u_n,u_n \rangle \end{bmatrix} . \tag{10}$$

In this case G_{2n+1} has only pure real elements. If G_{2n+1} is also singular, the following relation holds among the cofactors:

$$\frac{\Delta_{pq}}{\Delta_{pp}} = \sqrt{\frac{\Delta_{qq}}{\Delta_{pp}}} . \tag{11}$$

This relation is proved in the Appendix. The pencil-of-functions method assumes that G_{2n+1} is singular and makes use of (8), (9), and (11) to

form the following characteristic equation for the process:

$$\sqrt{\frac{\Delta_{00}}{\Delta_{00}}}\ s^n + \sqrt{\frac{\Delta_{11}}{\Delta_{00}}}\ s^{n-1} + \cdots + \sqrt{\frac{\Delta_{nn}}{\Delta_{00}}} = 0 \quad . \tag{12}$$

It may be shown that, in general, G_{2n+1} is nonsingular because y cannot be expressed as a linear combination of the y_i and u_i under the following conditions of imperfect modeling:

1. y has a random noise component.

2. The model order, n, is less than the order of

    the process or waveform being modeled.

3. Both 1 and 2.

If any of the above conditions apply the set of functions,

$$S = \left\{ y,\ y_1,\ \cdots,\ y_n,\ u_1,\ \cdots,\ u_n \right\} \quad ,$$

is linearly independent, and due to this fact, the Gram matrix [27], G_{2n+1}, formed from those functions of S is nonsingular. Otherwise, for conditions of perfect modeling, the functions of S are linearly dependent, G_{2n+1} is singular, and (11) holds.

Thus, if the process can be modeled perfectly, that is, with no error, then (12) is equivalent to (8). However, if the process cannot be modeled perfectly, (11) no longer holds and (12) becomes less accurate than (8) for estimating the parameters of the approximate model. Since the parameter values of the approximate model are transplanted into the true model, it is not clear if the α_i or the $\sqrt{\Delta_{ii}/\Delta_{oo}}$ more accurately portray the process after this transplant. In the next section numerical evidence is presented that indicates that the α_i provide better estimates. However, since the α_i and the $\sqrt{\Delta_{ii}/\Delta_{oo}}$ are computed in extremely different ways, the results may not indicate the true situation due to inaccuracies in computation.

Aside from the problem mentioned above the pencil-of-functions method has two other difficulties of which only one has a simple remedy.

The difficulty that has a simple remedy is related to the use of integrators for the filters within the system model. The continuous-time integrators cannot be implemented exactly by any algorithm. When approximate integrators are cascaded as they are in the pencil-of-functions method, large errors accumulate quickly and the intended result destroyed after a number of integrations.[*] This difficulty can be resolved by cascading discrete integrators to obtain filters with pulse transfer functions given by

$$F_i = F_i(z) = \left(\frac{z}{z-1}\right)^i = \left(\frac{1}{Z}\right)^i$$

which can be implemented on a digital computer with no error by using the difference equations:

$$y_i(k) = y_i(k-1) + y_{i-1}(k)$$

and $\quad u_i(k) = u_i(k-1) + u_{i-1}(k)$.

The variable Z is defined as

$$Z = 1 - \frac{1}{z} \quad ,$$

and z is the z-transform variable. When discrete integrators are used the _discrete_ pencil-of-functions method results. The poles of the pulse transfer function of the process may be estimated as

---

[*]This feature of the pencil-of-functions method has been consistently observed in numerical implementations. This encroachment of systematic error is inconsistent with generally accepted interpretation of numerical integration processes and has not been explained analytically, to date.

$$z_i = \frac{1}{1-Z_i}$$

where Z_i is the ith zero of

$$1Z^n + \alpha_1 Z^{n-1} + \cdots + \alpha_n = 0 \tag{13}$$

and the α_i are found by use of equation (4).

If the continuous inner product (6e) is replaced with the discrete inner product,

$$\left\langle X_1, X_2 \right\rangle^D = \sum_{k=0}^{M-1} X_1^*(k) \, X_2(k) \quad . \tag{14}$$

It can be shown that $\underline{r}^D = \Omega'\underline{y}$ and $G_{2n}^D = \Omega'\Omega$ where G_{2n}^D and $\underline{r}^D$ are formed with the discrete inner product (14) in the same way that G_{2n} and $\underline{r}$ are formed with the continuous inner product (6e). Then,

$$\alpha_i = \frac{\Delta_{0i}^D}{\Delta_{00}^D} \tag{15}$$

where Δ_{pq}^D denotes the cofactor formed by deleting row p+1 and column q+1 of G_{2n+1}^D, and G_{2n+1}^D is the Gram matrix formed with the discrete inner product in the same way G_{2n+1} is formed with the continuous inner product. Equation (15) follows from Cramer's rule in the same way equation (9) does. As before the relation,

$$\frac{\Delta_{pq}^D}{\Delta_{pp}^D} = \sqrt{\frac{\Delta_{qq}^D}{\Delta_{pp}^D}} \tag{16}$$

holds if G_{2n+1}^D is singular. Combining (13), (15), and (16) yields the characteristic equation of the system:

$$\sqrt{\frac{\Delta_{00}^D}{\Delta_{00}^D}} \, Z^n + \sqrt{\frac{\Delta_{11}^D}{\Delta_{00}^D}} \, Z^{n-1} + \cdots + \sqrt{\frac{\Delta_{nn}^D}{\Delta_{00}^D}} = 0 \quad . \tag{17}$$

Equation (17) is the equivalent of (12) for the discrete method. The choice of positive radicals in (17) follows from arguments counterpart to those put forth by Jain [19] for the continuous case.

Estimates of the poles of the Laplace transfer function of the process, s_i, are related to the zeros of (13) and (17) by

$$s_i = -\frac{\ln(1-Z_i)}{T} \quad .$$

In the next section the discrete version of the pencil-of-functions method is tested on noisy data and the performance of equation (13) is compared to that of (17) in order to demonstrate the superiority of (13) in estimating the system poles.

Now attention is turned to the second difficulty with the method that does not have a simple remedy. This difficulty is related to the attenuation of the higher frequency modes of the process output by the repeated integrations applied to the output waveform. It can be verified that an integrator is simply a first order filter whose Laplace transfer function has a pole at the origin in the s-plane. Such a filter tends to suppress the higher frequencies present at its input. The higher frequency suppression phenomenon is illustrated in Figure 3. Normally, when an exponential function is integrated repeatedly, components consisting of powers of time exist in the higher integrals as well as the original exponential function components. In Figure 3 the components of powers of time have been subtracted from the integrated waveforms in order to make the attenuation of the higher modes more evident. The first waveform is a hypothetical waveform provided for analysis. The waveforms that follow are the integrals of increasing order of the first waveform and display the increasing dominance of the fundamental mode or the mode of lowest frequency.
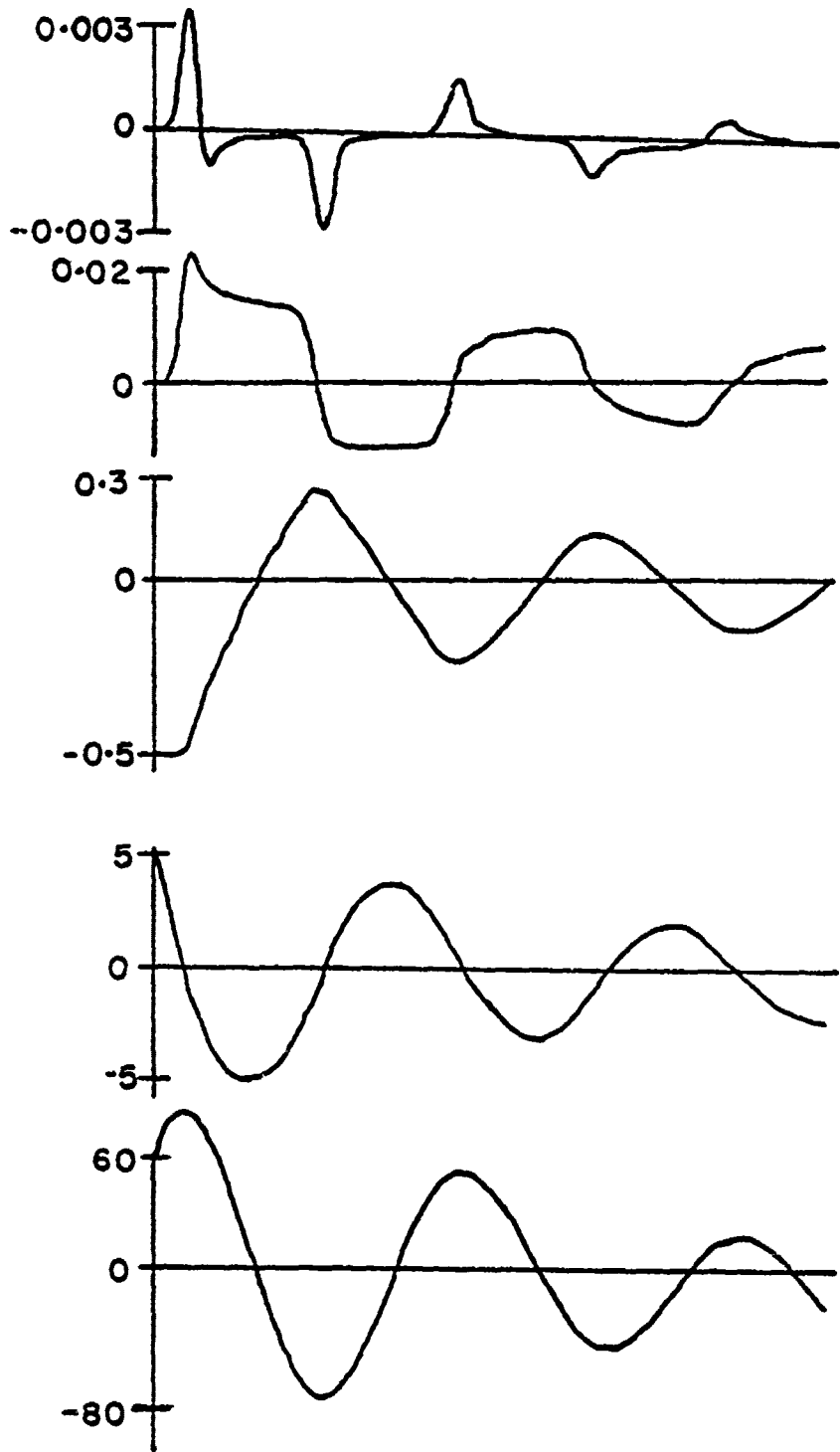
Figure 3. Successive integrals of a hypothetical waveform.

Further integrations yield nearly identical waveforms. The integrated waveforms tend to become linearly dependent at higher model orders. The Gram matrix, G_{2n} or G_{2n}^D, then tends to singularity and the method becomes unstable. The suppression phenomenon occurs in both the discrete and continuous methods. In fact, even for very modest model orders, the method can become numerically ill-conditioned to a degree that special care must be taken to assure accurate inversion of G_{2n} or G_{2n}^D. The examples of the next section illustrate the increasing ill-condition with increasing model order by computing the condition number of G_{2n}^D.

3.4 Numerical Examples of the Pencil-of-Functions Method

In the first example, impulse input to the system is assumed and the discrete method is applied in the analysis of a waveform consisting of 50 samples defined by:

$$y(k) = \sum_{j=1}^{4} A_j e^{s_j kT} + n(k) \qquad k = 0,1,\cdots,49$$

where $A_1 = 1,$ $s_1 = -1 + j10,$

$A_2 = 1,$ $s_2 = -1 - j10,$

$A_3 = 1,$ $s_3 = -1.5 + j30,$

$A_4 = 1,$ $s_4 = -1.5 - j30,$

$n(k)$ is a Gaussian distributed white noise sequence of 50 samples, and $T = 1/49$. The signal-to-noise ratio is 30 dB, where signal-to-noise ratio (SNR) is defined by:

$$SNR \ (dB) = 20 \ \log_{10} \frac{\delta}{2\sigma} \tag{18}$$

$$\text{and} \quad \delta = \max_{k} \left| \sum_{j=1}^{4} A_j e^{s_j kT} \right| \qquad \text{(maximum magnitude of uncorrupted waveform)}$$

σ = standard deviation of noise.

Four poles are requested. Thirty Monte Carlo runs are made where each run uses a different noise sequence. Figure 4 shows the resulting s-plane pole estimate for all Monte Carlo runs overlaid onto a common plot. In Figure 4(a), the poles are estimated with the roots of equation (17), and in Figure 4(b), the poles are estimated with the roots of equation (13). The reader is reminded that the residues of both poles are of unit amplitude thus leading to the conclusion that the apparent deterioration of pole accuracy with increasing frequency is an artifice of the process.

In the second example the same analysis is carried out for a higher model order. The waveform is given by:

$$y(k) = \sum_{j=1}^{6} A_j e^{s_j kT} + n(k) , \qquad k = 0,1,\cdots,49 ,$$

where $A_5 = 1,$ $s_5 = -2 + j50,$

   $A_6 = 1,$ $s_6 = -2 - j50,$

and all other details remain unchanged from the first example. Six poles are requested. Figure 5 shows the resulting S-plane pole estimates. In Figure 5(a) the poles are estimated with the roots of (17), and in Figure 5(b) the poles are estimated with the roots of (13).

The condition number of G_{2n}^{D} is averaged over the thirty Monte Carlo runs and displayed in Figures 4 and 5. The condition number is defined by [28]:

condition number = 6.6×10^6

s-plane

jω

σ

(a)

s-plane

jω

σ

(b)
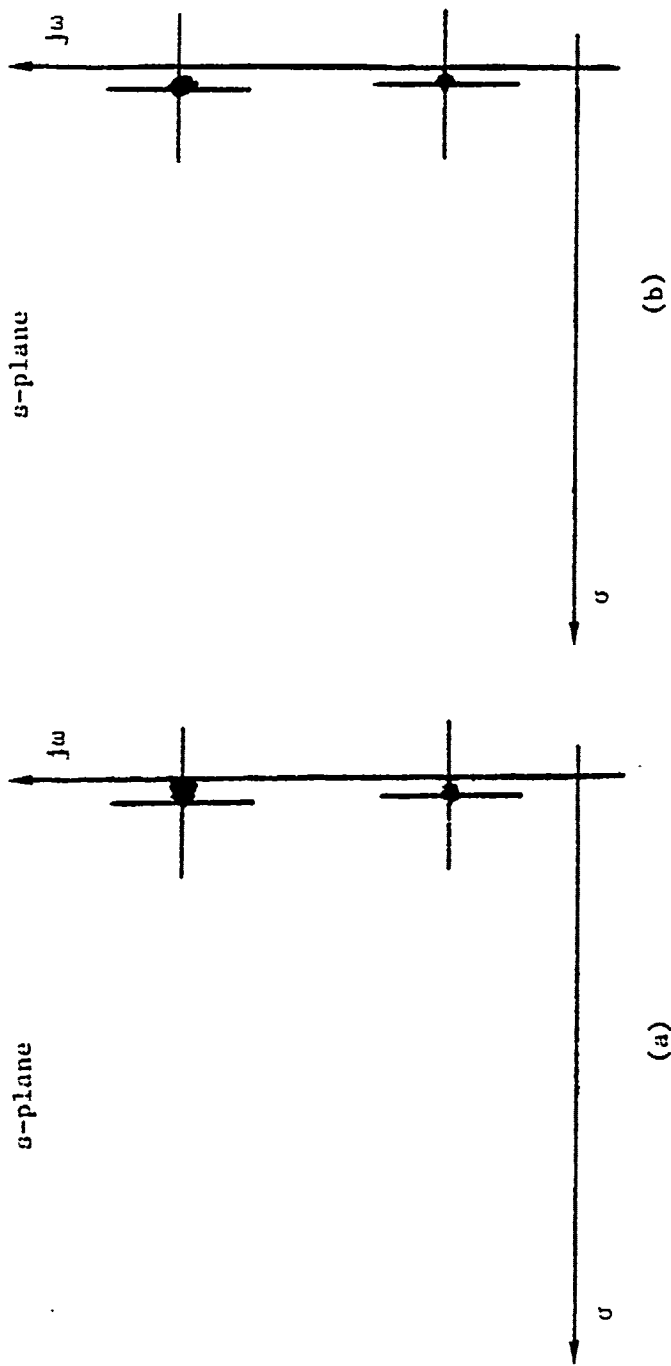
Figure 4.   Overlay plot of pole estimates of a fourth-order system.
(a) estimates using roots of (17),
(b) estimates using roots of (13).

condition number = 2×10^{13}
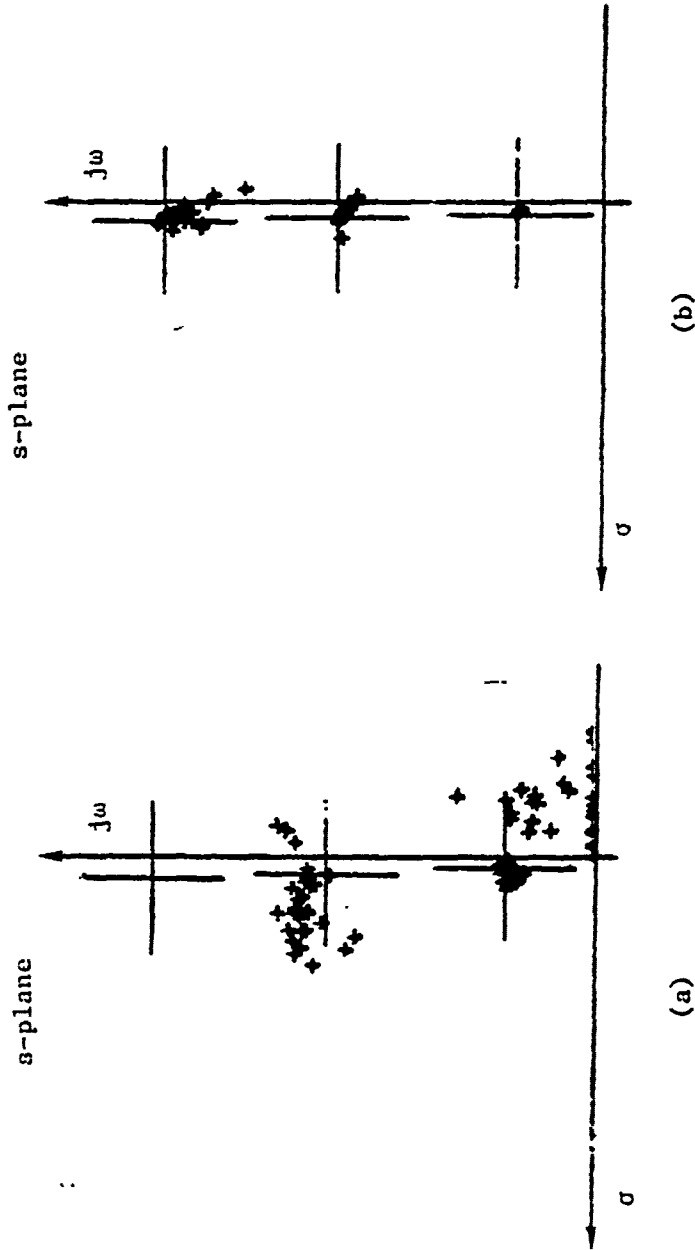
Figure 5. Overlay plot of pole estimates of sixth-order system.
(a) estimates using roots of (17),
(b) estimates using roots of (13).

$$\text{Condition number} = ||G_{2n}^D|| \ ||[G_{2n}^D]^{-1}||$$

where $||\cdot||$ denotes the Chebyshev matrix norm defined by:

$$||A|| = \frac{\max}{1 \leq i \leq N} \sum_{j=1}^{N} |a_{ij}|$$

and a_{ij} is the element of the ith row and j^{th} column of the N-dimensional matrix A. The larger the condition number, the more ill-conditioned the matrix A.

The results of these examples demonstrate that better pole estimates are obtained by using (13) instead of (17). The increasing condition number from the first to the second example indicate that the method is becoming rapidly ill-conditioned as the order of the method is increased. The results of a third example for which an eighth order method was used to analyze a noise corrupted waveform composed of eight exponential components are not presented because the method became so ill-conditioned that the intended result was completely destroyed.

It was found that the pencil-of-functions method becomes ill-conditioned for the analysis of waveforms containing many poles. Even though the results of these examples do not apply to the continuous version of the method directly, it is known that in the limit as T approaches zero the discrete method approaches the continuous method, and hence, there is a measure of similarity in the two methods. This measure of similarity is felt to be sufficient to claim that the continuous version of the method becomes ill-conditioned at higher order.

Chapter IV

THE ADAPTIVE METHOD

4.1 Introduction

The adaptive method is an iterative method which is quite tolerant

of noise in the waveform undergoing exponential analysis. The original

idea for this method was inspired by the pencil-of-functions concept

due to Jain [17]. In this chapter, the adaptive method is derived, not

from the pencil-of-functions concept as it was originally, but rather

from the parametric models of Chapter II. Formulating the method in

this way is not only simpler but yields greater insight into the

method's nature.

4.2 An Adaptive Filtering Scheme

The adaptive method results from the identification scheme of

Chapter II under the following assumptions:

1. $\alpha_o = 1$.

2. $F_i = \dfrac{z}{z-z_i}$.

3. The model input is a unit sample at $k = 0$ (discrete
   impulse).

The unique feature of the method is that the filter poles, z_i, may be

adjusted to any value in the z-plane. An adaptive technique for ad-

justing the filters consists of first initializing the filters to

arbitrary values in the z-plane and repeating the following steps:

1. Find an estimate of the process transfer function using the current filters in the model.

2. Set each filter pole to one pole of the estimated transfer function.

This process is repeated until the α_i approach zero.

It is shown in the next section that the poles of the process can be estimated during the course of iteration by

$$\hat{z}_i = \frac{z_i}{1 + \alpha_i} \qquad (19)$$

removing the need for finding the roots of a polynomial. The filter poles are updated to $\hat{z}_i$ on each iteration. When the α_i approach zero, the pole updating ceases and the method converges. At each iteration, the α_i are found by using equation (4). At convergence the s-plane poles, s_i, can be obtained from the filter poles by

$$s_i = \frac{\ln z_i}{T} , \qquad (20)$$

and the $A_i = \beta_i$.

4.3 Estimation of Process Poles from Transfer Function Parameters

As usual, the poles of the process transfer function can be estimated as the poles of (3). However, to estimate the poles, a polynomial in z is needed. To find this polynomial the numerator and denominator of (3) are multiplied by the product of all filter denominators, that is, by $\prod_{i=1}^{n} (z-z_i)$. The required polynomial is the denominator of the expression that results after the multiplications

indicated above are carried out and terms of equal degree have been combined in the denominator. Although it can be done, the formulation of the polynomial coefficients on a digital computer requires some small computational burden. But another method exists for estimating the poles that bypasses this complication as well as the necessity for finding the roots of a polynomial. For the sake of discussion, assume that the filter poles have been adjusted to nearly coincide with the process poles and examine the behavior of the $(i+1)^{th}$ term of the denominator of (3) when the variable z approaches the value of the ith process pole. It is observed that the $(i+1)^{th}$ term can become arbitrarily large if the ith filter pole is arbitrarily close to the ith process pole. It is then possible to write a simplified expression for the denominator of (3) which is approximately equivalent when z is equal to the ith process pole, viz.,

$$1 + \frac{\alpha_i z}{z - z_i} , \qquad (21)$$

where all other terms other than the $(i+1)^{th}$ term in the denominator of (3) are negligibly small. If

$$1 + \frac{\alpha_i \hat{z}_i}{\hat{z}_i - z_i} = 0 \qquad (22)$$

where $\hat{z}_i$ is the value of z for which the equality holds, then $\hat{z}_i$ is a reasonable estimate of the ith process pole. Equation (19) is obtained by solving (22) for $\hat{z}_i$. The approximations of (21) and (22) follow from observing that near convergence of the z_i all of the α_i except α_o, which is fixed as unity, vanish. Therefore, the α_o term dominates along with the $(i+1)^{th}$ term as argued above.

4.4 Numerical Examples of the Adaptive Method

The first example of the adaptive method uses a simple first-order model to analyze a sequence consisting of three samples. Because of the example's simplicity, hand calculations and concrete numbers can be displayed.

The sequence to be analyzed is

$$\{y(k), \ k=0,1,2\} = \{2,1,2\} \quad .$$

It can be shown that

$$y_m(k) = \frac{5}{3} \quad \text{(a constant sequence)}$$

minimizes the mean-squared error between y and y_m if the problem is restricted to a first-order solution. Therefore, the expected results of this analysis after the adaptive method converges are: $A_1 = \frac{5}{3}$ and $z_1 = 1$. Let the initial filter pole, z_1, be set to one. One might expect that the method would be convergent immediately in this case. However, the method, in fact, will not converge at this value of z_1 due to the error introduced by the use of the approximate model. The convergent value of z_1 should be slightly perturbed from the expected value.

The estimator of equation (4) is applied to obtain estimates of α_1 and β_1. In this case,

$$\Omega = \begin{bmatrix} 2 & 1 \\ 3 & 1 \\ 5 & 1 \end{bmatrix} \ ,$$

and the system that must be solved is

$$\begin{bmatrix} 38 & 10 \\ 10 & 3 \end{bmatrix} \begin{bmatrix} -\alpha_1 \\ \beta_1 \end{bmatrix} = \begin{bmatrix} 17 \\ 5 \end{bmatrix} .$$

The estimates are $\alpha_1 = -1/14 \approx -.07143$ and $\beta_1 = 20/14 \approx 1.429$. The estimate of the process pole is

$$\hat{z}_1 = \frac{z_1}{1+\alpha_1} = \frac{1}{1-1/14} = \frac{14}{13} \approx 1.077.$$

The estimates above constitute the results of the first iteration. For the second iteration the filter pole is updated to 1.077 and the same procedure is repeated for iterations two through five. The results for all iterations are displayed in Table 1.

Next, the iterative scheme for the actual model set forth in Chapter II is simultaneously combined with the adaptive filtering scheme and is applied to correct the biased value just obtained with the approximate model. An initial estimate of the process transfer function is required to start this estimation procedure. The parameters obtained with the approximate model at convergence are used to form this initial estimate. The initial pole is 1.077. The most recent model output sequence is computed for the nth order case by using the following difference equations in the order indicated:

$$u_i(k) = u(k) + z_i u_i(k-1),$$

$$y_m(k) = \frac{\sum_{i=1}^{n} (\beta_i u_i(k) - \alpha_i z_i y_{mi}(k-1))}{1 + \sum_{i=1}^{n} \alpha_i} ,$$

Table 1   Estimates using the approximate model.

Iteration number	$-\alpha_1$	β_1	z_1
1	7.143×10^{-2}	1.429	1.077
2	2.711×10^{-4}	1.539	1.077
3	2.279×10^{-6}	1.539	1.077
4	-4.245×10^{-7}	1.539	1.077
5	2.954×10^{-7}	1.539	1.077

Table 2   Sequences on the first iteration of the estimation scheme
for the actual model.

k	$u_1(k)$	$y_m(k)$	$y_{m1}(k)$
0	1	1.539	1.539
1	1.077	1.658	3.316
2	1.160	1.785	5.356

$$y_{mi}(k) = y_m(k) + z_i y_{mi}(k-1).$$

These equations are valid for the nth order model. For the first

order ($n=1$, $i=1$) model that is considered here, the equations are

$$u_1(k) = u(k) + z_1 u_1(k-1),$$

$$y_m(k) = \frac{\beta_1 u_1(k) - \alpha_1 z_1 y_{m1}(k-1)}{1 + \alpha_1},$$

$$y_{m1}(k) = y_m(k) + z_1 y_{m1}(k-1),$$

and are used to compute the results shown in Table 2. From the results

of Table 2,

$$\Omega = \begin{bmatrix} 1.539 & 1.000 \\ 3.316 & 1.077 \\ 5.356 & 1.160 \end{bmatrix},$$

and the system which must be solved is

$$\begin{bmatrix} 42.051 & 11.323 \\ 11.323 & 3.506 \end{bmatrix} \begin{bmatrix} -\alpha_1 \\ \beta_1 \end{bmatrix} = \begin{bmatrix} 17.106 \\ 5.397 \end{bmatrix}.$$

The estimates are $\alpha_1 \simeq +5.973 \times 10^{-2}$ and $\beta_1 \simeq 1.732$. The estimate of

the process pole is

$$\hat{z}_1 = \frac{z_1}{1 + \alpha_1} \simeq \frac{1.077}{1 + .05973} \simeq 1.017.$$

The estimates just found constitute the results of the first itera-

tion using the estimation scheme for the actual model. The filter

pole is updated to 1.017 and the same procedure is repeated several

more times to obtain the results shown in Table 3.

The results in Table 3 indicate that the estimation procedure for

the actual model has indeed converged to the expected parameter values

Table 3   Estimates u— · he actual model.

Iteration number	$-\alpha_1$	β_1	z_1
1	-5.973×10^{-2}	1.732	1.017
2	-2.053×10^{-2}	1.705	.996
3	1.163×10^{-3}	1.669	.997
4	2.349×10^{-3}	1.663	1.000
5	5.878×10^{-4}	1.665	1.000
6	-5.633×10^{-5}	1.667	1.000
7	-7.576×10^{-5}	1.667	1.000
8	-1.697×10^{-5}	1.667	1.000
9	2.032×10^{-6}	1.667	1.000
10	2.346×10^{-6}	1.667	1.000
11	9.632×10^{-7}	1.667	1.000
12	-2.289×10^{-7}	1.667	1.000
13	-1.717×10^{-7}	1.667	1.000
14	2.861×10^{-8}	1.667	1.000

whereas the results in Table 1 clearly show that the procedure for the approximate model does not. However, the magnitude of the error that the use of the approximate model introduces in the estimated pole value is relatively small.

The results of the next example provide further evidence that, indeed, the error in the parameter estimates are small when adaptive filters are used in the approximate model.

To illustrate the performance of the adaptive method on measured data, the method was applied in the extraction of the natural resonance of the electrical transient response of a thin cylinder in free space. Figure 6 shows the responses of the cylinder at five points along its length which were measured by techniques described in reference [29]. The cylinder was excited by a 500 picosecond burst of radiation that is normally incident to its axis. The cylinder of 60 centimeters long and approximately 1 centimeter in diameter. The waveform consists of 512 samples and has a time step of $.9775 \times 10^{-11}$ seconds. The first 109 samples are ignored since the forcing wavefront impinging on the cylinder corrupts this portion of the natural response. The preprocessing increment is 10 samples. This means that every 10 adjacent samples are averaged to form one sample of the preprocessed waveform beginning at sample 110. The preprocessed waveform then has the integer portion of $(512-109)/10$ or 40 samples with a time step of $(10) \cdot (.0775 \times 10^{-11}) = .9775 \times 10^{-10}$ seconds. The estimation procedures for both the approximate model and the actual model were applied to the preprocessed

waveforms and the results for each case is shown in Figure 7. The
extracted poles from all responses are shown overlaid in Figure 7.
Although the data appear to be free of noise, the signal to noise
ratio is estimated to be between 15 dB and 20 dB by observing the
model error. The noise is thought to arise from such phenomenon
as reflections on the transient range and in the probe cabling al-
though no tests were made to confirm this. It should be pointed
out that the poles obtained with the actual model actually minimize
the mean-squared error, and therefore provide the best least-squares
fit to the preprocessed responses. If better parameter estimates are
to be found, more must be known about the noise that corrupts the
waveforms. It is interesting to note that the results obtained with
the approximate model and those obtained with the actual model are
almost identical. One has to strain to see the difference. Many
other cases have been studied whose results have confirmed the trend
of nearly identical pole estimates. In many practical cases, one may
choose to use the results from the approximate model without bothering
to refine those estimates further by using the estimation procedure
for the actual model. This may be a wise choice, particularly in view
of the fact that the adaptive estimation procedure for the actual
model does not converge in many cases where the adaptive procedure
for the approximate model does converge.

In the next several examples, the analysis of numerically generated
transient data is examined. The transient data were obtained using
the time domain computer code TWTD [30]. The structure modeled by
TWTD was a thin cylindrical scatterer. This structure was chosen
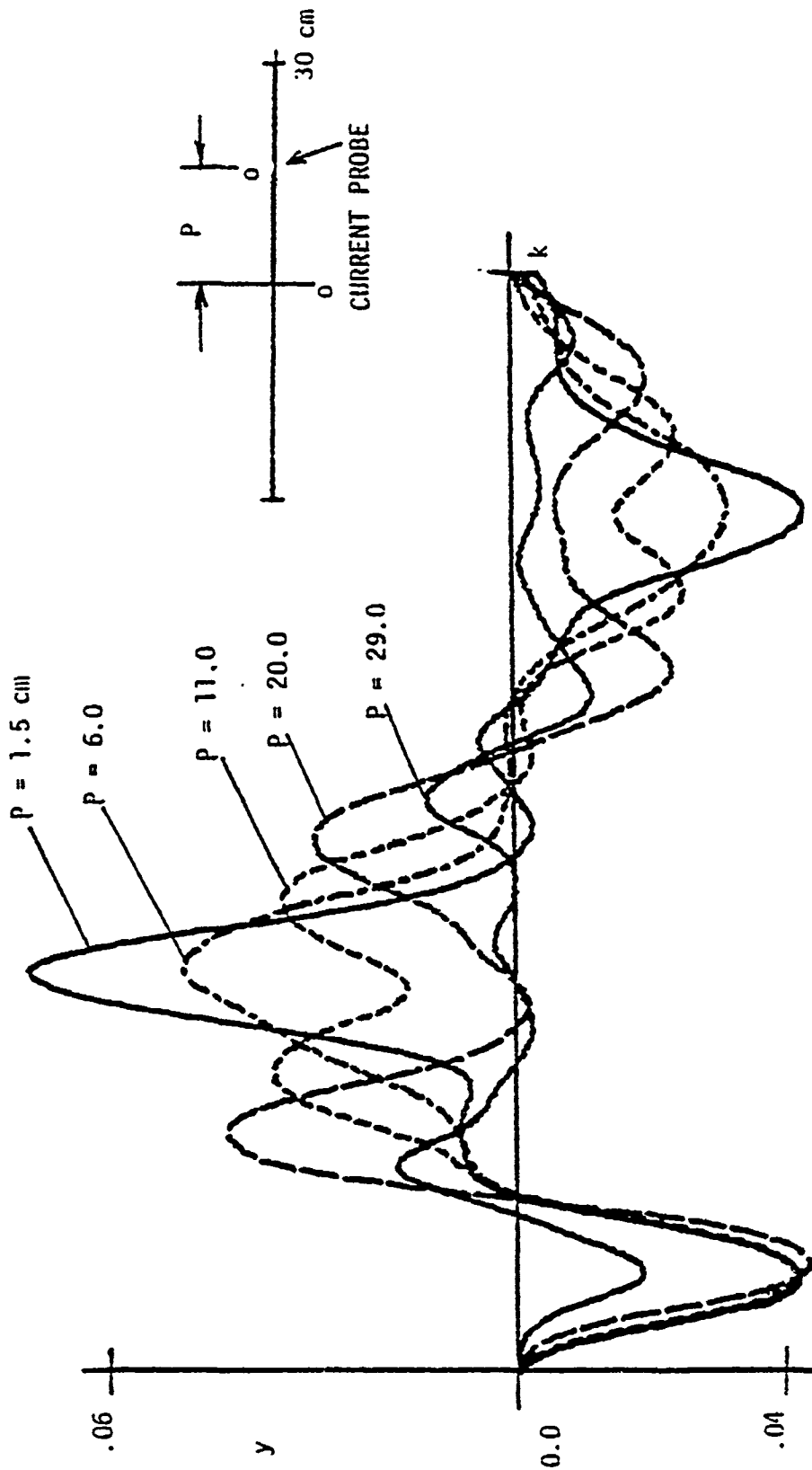
Figure 6   Transient responses measured at five points along the 60 centimeter cylinder.

ACTUAL MODEL

True: -.220 + j 6.800
Average: -.252 + j 6.66
Radius: .162

True: -.188 + j 4.835
Average: -.298 + j 4.733
Radius: .315

True: -.147 + j 2.874
Average: -.232 + j 2.899
Radius: .206

True: -.082 + j .926
Average: -.044 + j .913
Radius: .082

APPROXIMATE MODEL

True: -.220 + j 6.800
Average: -.219 + j 6.689
Radius: .184

True: -.188 + j 4.835
Average: -.278 + j 4.748
Radius: .271

True: -.147 + j 2.874
Average: -.226 + j 2.903
Radius: .195

True: -.082 + j .926
Average: -.043 + j .913
Radius: .083

L = .6 meters
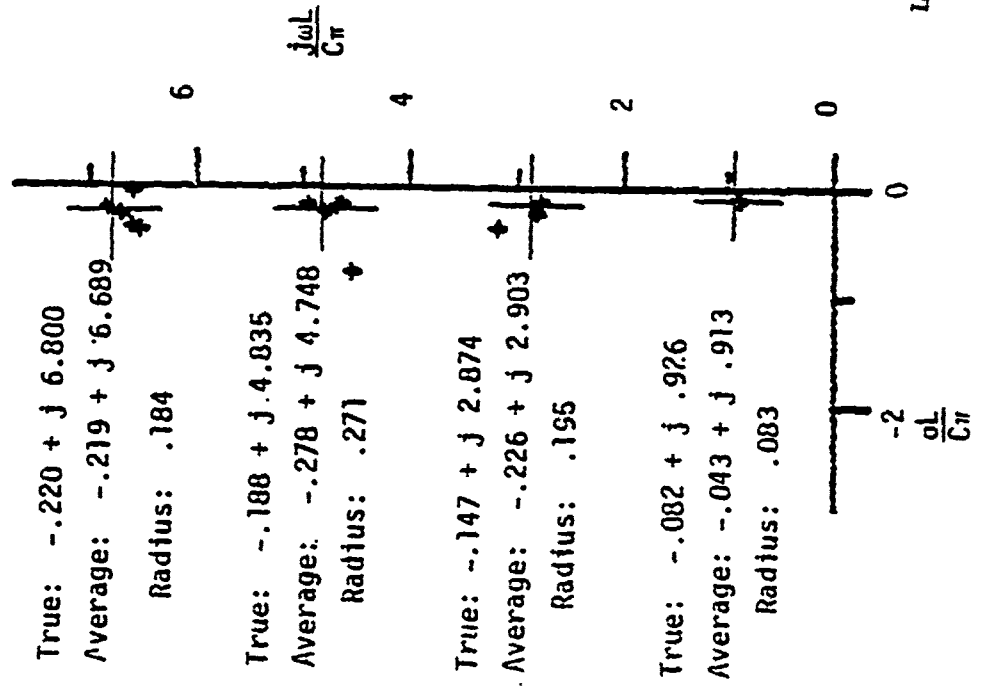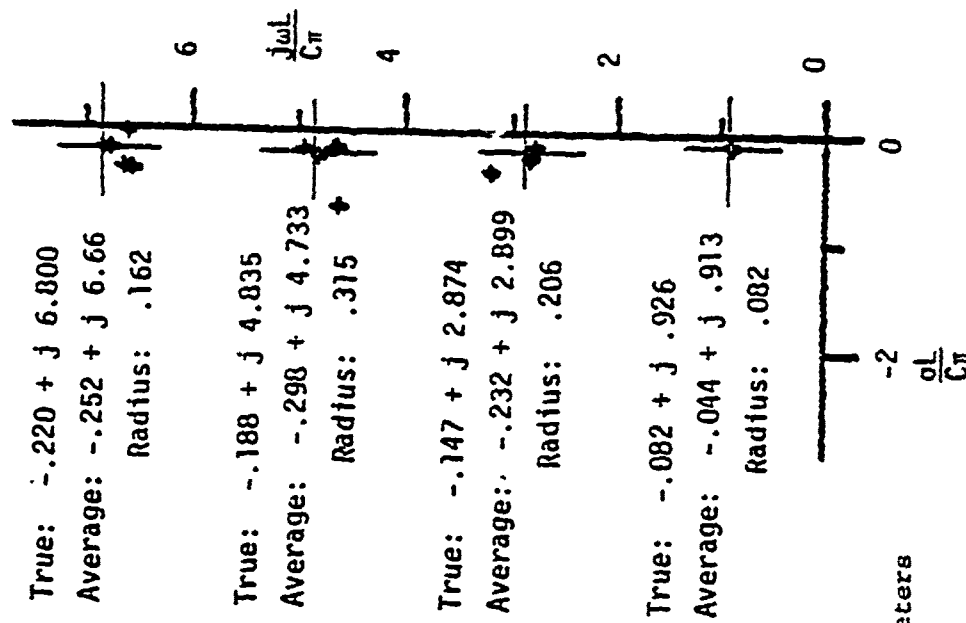
Figure 7   Poles for the measured cylinder data. The large crosses represent
numerical SEM results for the structure as computed by Tesche [31].

because of the availability of comparative results obtained by Tesche
[31]. The true pole values for the first six odd harmonic modes
of the cylinder obtained by Tesche with an integral equation technique
are listed in Table 4. These values are the theoretical values which
are used for comparison in the examples that follow.

The first three examples with the TWTD data illustrate the results
that can be obtained with the adaptive method at three different
signal-to-noise ratios (SNR): 25 dB, 20 dB, and 15 dB. Figure 8
illustrates a noise contaminated TWTD waveform consisting of 256 samples
with a 15 dB SNR where SNR is defined in the spirit of equation (8).
The time step is 0.68020×10^{-10} seconds. The waveform is that of the
current versus time history at the center of a one-meter cylinder which
is excited by a voltage source offset approximately 15 centimeters from
the center. The voltage source has a Gaussian-pulse time history where
pulse width referred to the 1/e level of the function is approximately .6
nancseconds.   Although the cylinder has an infinite number of modes,
only the first four low frequency modes dominate the response since
the excitation is band limited. Figure 9 shows the results of the
estimation procedures for both the actual model and the approximate
model for five Monte Carlo runs where each run uses a different
noise sequence. The noise is Gaussian distributed and uncorrelated.
The first 60 samples are ignored to exclude the influence of the driv-
ing voltage. The waveforms are preprocessed before being analyzed
with a preprocessing increment of 5 samples beginning at sample 70.

Table 4   Cylinder pole values predicted by Tesche [31]

	sL/c
Real	Imag
-0.082	0.926
-0.147	2.874
-0.188	4.835
-0.220	6.800
-0.247	8.767
-0.270	10.733

Figures 10 and 11 show the pole estimates for the same data with SNR's
of 20 and 25 dB, respectively. Tables 5 and 6 tabulate the pole
values corresponding to Figure 9; Tables 7 and 8 correspond to Figure
10; and Tables 9 and 10 correspond to Figure 11.

Several things should be pointed out about these results. First,
even though there are four dominate modes in the data only three pole
pairs are requested for the 15 and 20 dB cases. Only three pole pairs
are requested because the eighth order method often diverges. In
several of the Monte Carlo runs not all of the poles are in conjugate
pairs. However, most of the unmatched poles had values close to those
reported by Tesche. The runs which did not converge are so labeled.
Nonconvergent runs usually produce pole estimates that differ dras-
tically from Tesche's results. Hence, a reasonable procedure to
handle the case where the method converges but yields unmatched poles
might be to simply assume that each unmatched pole possesses a con-
jugate companion pole. In fact, a promising procedure to eliminate
this problem would be to increase the model order once for each un-
matched pole at convergence, introduce the appropriate conjugate pole,
and continue the iteration until, hopefully, convergence is achieved
with all poles occurring in conjugate pairs.

For the 25 dB case four pole pairs are requested and four con-
jugate pole pairs converged in each case except one which diverged.

The results for the offset-driven data indicate that the adaptive
method is able to provide useful results even in noise levels of
around 15 dB and even if the convergent poles are not in conjugate
pairs.

In the next two examples the adaptive method is applied in the analysis of the noise contaminated TWTD data, the current at the center of a one-meter cylinder. The exciting voltage generator has a Gaussian time history with a pulse width at the 1/e level of approximately .3 nanoseconds. Hence, the center-driven waveform contains components which are higher in frequency than the offset-driven waveform. Figure 12 displays the noise-contaminated center-driven waveform with a 20 dB SNR. The noise is Gaussian distributed and uncorrelated. The first 69 samples are ignored to exclude the influence of the driving voltage. The waveforms are preprocessed before being analyzed with a preprocessing increment of 5 samples, beginning at sample 70. Figures 13 and 14 show the pole estimates for the center-driven TWTD data with SNR's of 20 and 25 dB, respectively. Tables 11 and 12 tabulate the pole values corresponding to Figure 13; and Tables 13 and 14 correspond to Figure 14.

The results for the center-driven data display the sensitivity of the higher frequency modes to noise. This sensitivity is probably due to a lower relative degree of coupling to the higher frequency modes for the center-driven case. That is, the higher frequency modes are relatively weak for the center-driven case and are more easily corrupted by the noise. For the data with a 25 dB SNR five pole pairs are extracted with success. As usual, a few Monte Carlo runs diverged.
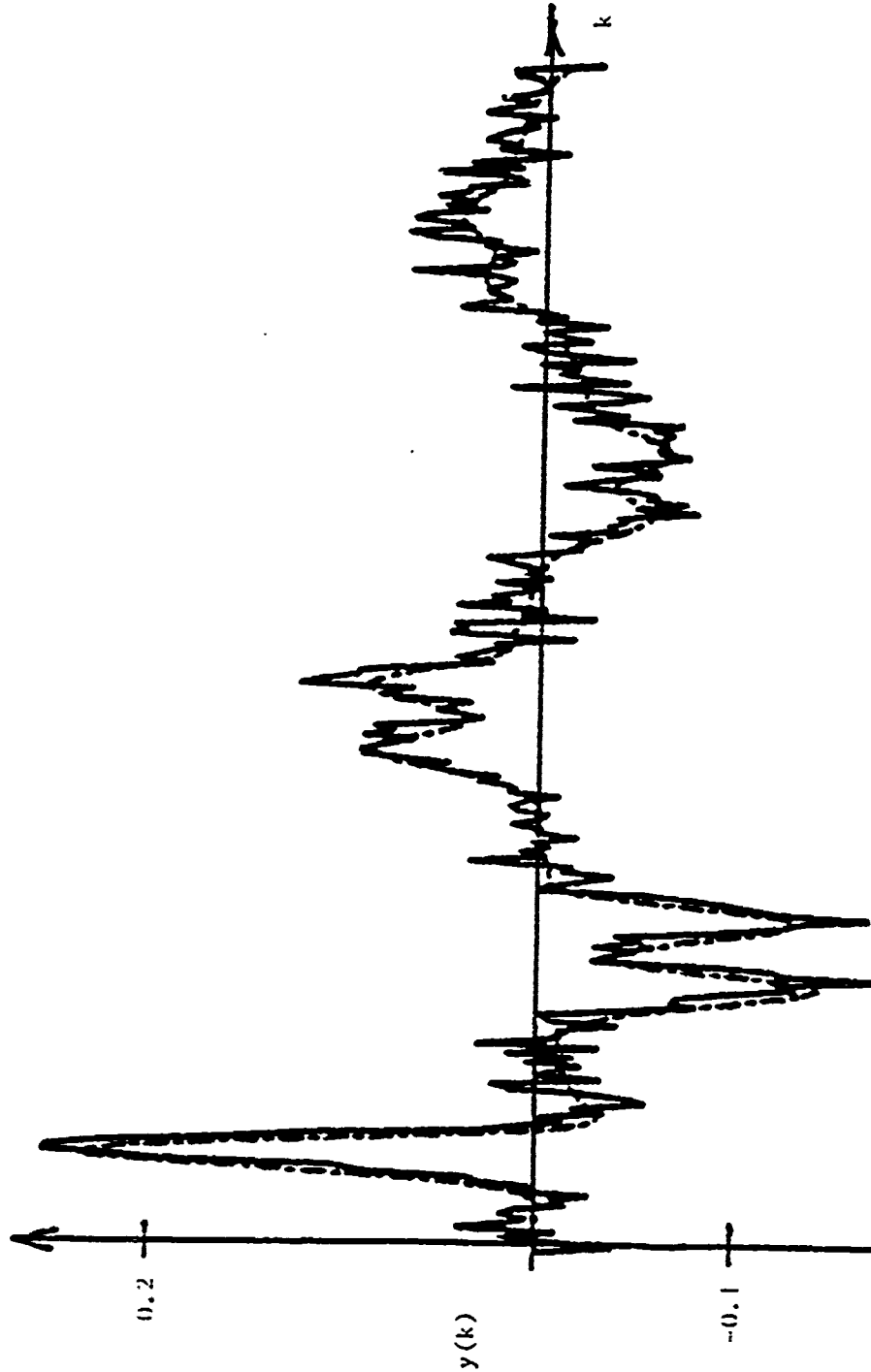
Figure 8   Noise-contaminated offset-driven TWT waveform, SNR=15 dB.   The uncontaminated waveform is plotted under the noisy waveform for comparison.

-46-

Figure 9   Poles for the offset-driven TWTD data, SNR = 15 dB.   The large
crosses indicate Tesche's values.

Table 5 Poles for the offset-driven TWTD data, SNR = 15 dB.
Results are for the approximate model.

Monte Carlo run:

1

Real	Imag
-.7949E-01	-4.770
-.1060E-01	2.997
-.2507	6.690
-.1414	4.777
-.9305E-01	-.8867
-.8887E-01	.9001

2

Real	Imag
-.1054	-4.726
-.8118E-01	-.9302
-.8140E-01	.9224
-.6230E-01	7.031
-.1093	4.702
-.5272E-01	-2.884

3

Real	Imag
-.2067	-4.750
-.1052	-2.929
-.1052	2.929
-.2067	4.750
-.7976E-01	.9072
-.7976E-01	-.9072

4

Real	Imag
-.9386E-01	-.8939
-.1513	4.799
.2405	9.330
-.1171	6.919
-.1641	-4.817
-.9407E-01	.8930

(non convergent)

5

Real	Imag
-.7123E-01	-4.804
-.9346E-01	.9212
-.5738E-01	6.761
-.1233E-01	4.845
-.9821E-01	-.9178
-.1402E-01	2.904

Table 6   Poles for the offset-driven TWTD data, SNR = 15 dB.
Results are for the actual model.

Monte Carlo run: 1

Real	Imag
-.1562	-4.724
-.2405	3.057
-.4036	6.619
-.1984	4.776
-.9289E-01	-.8775
-.8522E-01	.9037

(non convergent)

2

Real	Imag
-.1142	-4.733
-.8323E-01	-.9282
-.8049E-01	.9226
-.4474	6.677
-.1756	4.766
-.1450	-2.824

3

Real	Imag
-.4658	-4.585
-.1638	-2.924
-.1638	2.924
-.4658	4.585
-.8131E-01	.9069
-.8131E-01	-.9069

4

Real	Imag
-.9024E-01	-.8914
-.3003	4.823
.1161	8.785
-.2331	6.805
-.3548	-4.740
-.9013E-01	.8891

(non convergent)

5

Real	Imag
-9.844	4.313
-.6344E-01	.9139
-.8439E-01	6.761
-.5477E-01	4.928
-.7716E-01	-.8995
-.4314E-01	3.197

(non convergent)

Figure 10   Poles for the offset-driven TWTD data   SNR = 20 dB.   The large
crosses indicate Tesche's values.

-50-

Table 7　Poles for the offset-driven TWTD data, SNR = 20 dB.
Results are for the approximate model.

Monte Carlo run:

1		2		3	
Real	Imag	Real	Imag	Real	Imag
-.3007E-01	-6.730	-.1360	-4.774	-.1425	-6.802
-.2536	3.033	-.8348E-01	-.9141	-.1252E-03	2.917
-.2536	-3.033	-.2101	6.621	-.1536	6.824
-.3007E-01	6.730	-.2483	4.684	-.1811	4.794
-.1076	.9085	-.1031	-2.955	-.9304E-01	-.9009
-.1076	-.9085	-.8159E-01	.9114	-.9082E-01	.9062

4		5	
Real	Imag	Real	Imag
-.1494	-4.767	-.2158	-4.630
-.5572E-01	2.903	-.9754E-01	.9246
-.9923E-01	6.737	-.1542	6.802
-.1076	4.828	-.1599	4.727
-.9153E-01	-.9139	-.9714E-01	-.9116
-.8884E-01	.9213	-.1265	2.941

Table 8   Poles for the offset-driven TWTD data, SNR = 20 dB
Results are for the actual model.

Monte Carlo run: 1

Real	Imag
-.5311E-01	-6.774
-.5317	2.959
-.5317	-2.959
-.5311E-01	6.774
-.1129	.9111
-.1129	-.9111
(non convergent)	

2

Real	Imag
-.1623	-4.754
-.7921E-01	-.9070
-1.099	5.954
-.5390	5.032
-.1151	-2.890
-.7271E-01	.9138
(non convergent)	

3

Real	Imag
-.3033	-6.955
-.6217E-01	2.907
-.2997	6.738
-.2947	4.832
-.9164E-01	-.8941
-.8903E-01	.9086

4

Real	Imag
-2.866	-4.010
-.1220	2.835
-.9789E-01	6.723
-.9667E-01	4.866
-.6997E-01	-.9325
-.8585E-01	.9013
(non convergent)	

5

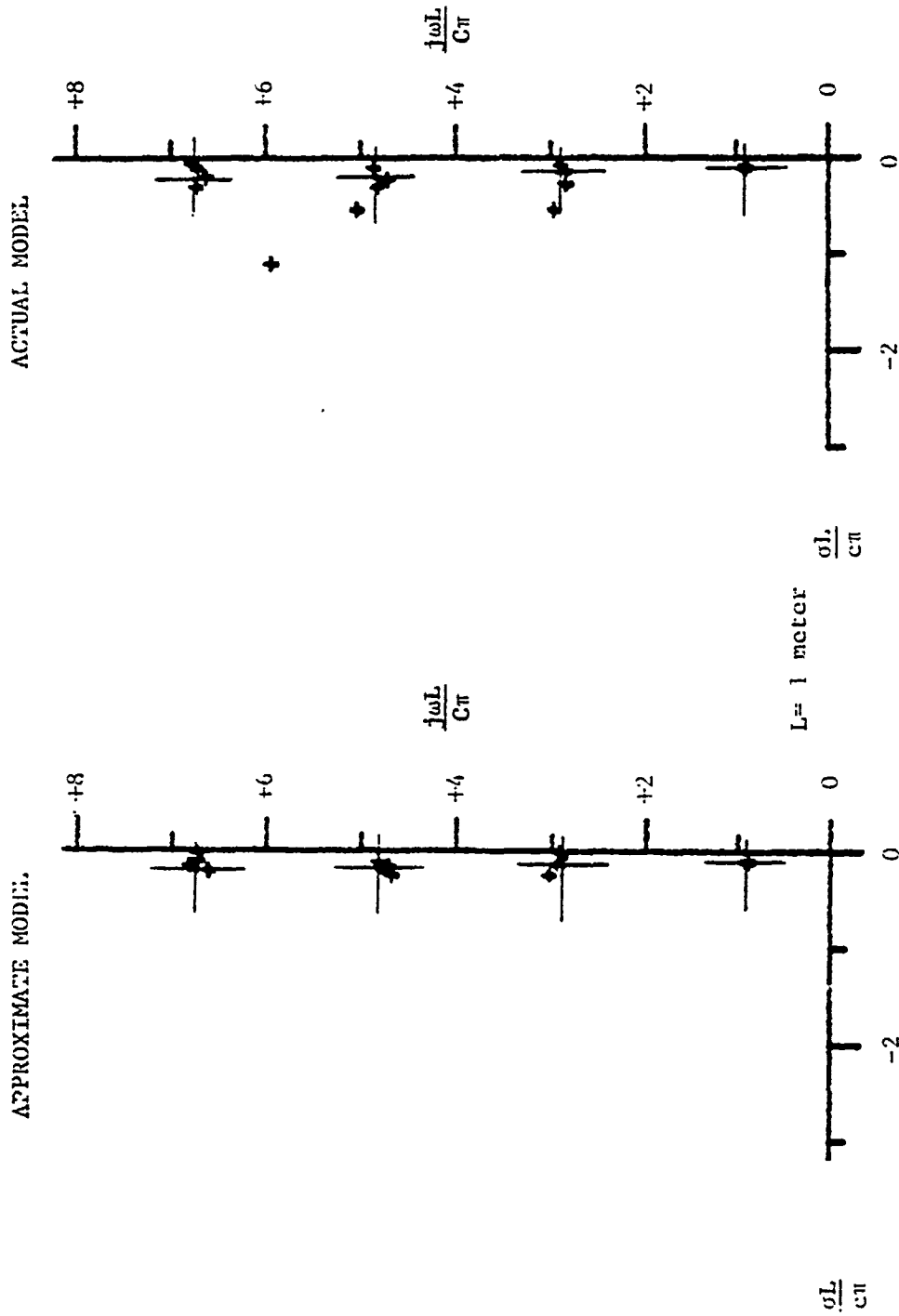| Real	Imag
-1.069	-3.461
-.1056	.9129
-.1879	6.630
-.2239	4.721
-.9713E-01	-.9299
-.2636	2.846
(non convergent)	

Figure 11   Poles for the offset-driven TWTD data, SNR = 25 dB.   The large
crosses indicate Tesche's values.

Table 9   Poles for the offset-driven TWTD data, SNR = 25 dB. Results are for the approximate model.

Monte Carlo run:

1		2		3	
Real	Imag	Real	Imag	Real	Imag
-.1898	-6.777	-.1515	-2.892	-.2644	-6.643
-.1560	2.841	-.1515	2.892	-.8274E-01	2.887
-.1898	6.777	-.1534	-6.705	-.2377	6.735
-.1560	-2.841	-.1579	4.902	-.1890	4.782
-.1785	-4.803	-.1579	-4.902	-.2450	-4.701
-.1785	4.803	-.9019E-01	-.9186	.8307E-01	-8.760
-.8871E-01	-.9151	-.1534	6.705	-.8269E-01	-.9139
-.8871E-01	.9151	-.9019E-01	.9186	-.8329E-01	.9157

4		5	
Real	Imag	Real	Imag
-.1867	-4.848	-.1622	-4.861
-.1460	2.885	-.8979E-01	-.9182
-.1813	-6.738	-.1789	6.744
-.1867	4.848	-.1789	-6.744
-.1460	-2.865	-.1636	-2.857
-.1813	6.738	-.1622	4.861
-.8258E-01	-.9178	-.1636	2.857
-.8258E-01	.9178	-.8979E-01	.9182

Table 10   Poles for the offset-driven TWTD data, SNR = 25 dB.   Results are for the actual model.

Monte Carlo run: 1

1

Real	Imag
-.2071	-6.749
-.1803	2.842
-.2071	6.749
-.1803	-2.842
-.1907	-4.804
-.1907	4.804
-.8928E-01	-.9152
-.8927E-01	.9152

2

Real	Imag
-.1636	-2.881
-.1636	2.881
-.1699	-6.690
-.1798	4.896
-.1798	-4.896
-.9039E-01	-.9185
-.1699	6.690
-.9039E-01	.9185

3

Real	Imag
-.3845	-6.791
-.1059	2.860
-.2659	6.747
-.2005	4.823
-.2770	-4.799
-.8069	-8.237
-.7948E-01	-.9122
-.8204E-01	.9127

(non convergent)

4

Real	Imag
-.2025	-4.850
-.1613	2.386
-.2011	-6.734
-.2025	4.850
-.1613	-2.886
-.2011	6.734
-.8263E-01	-.9176
-.8263E-01	.9176

5

Real	Imag
-.1755	-4.859
-.9007E-01	-.9183
-.1966	6.726
-.1966	-6.726
-.1743	-2.850
-.1755	4.859
-.1743	2.850
-.9007E-01	.9183

Figure 12   Noise-contaminated center-driven TWD waveform, SNR=20 dB.   The uncontaminated
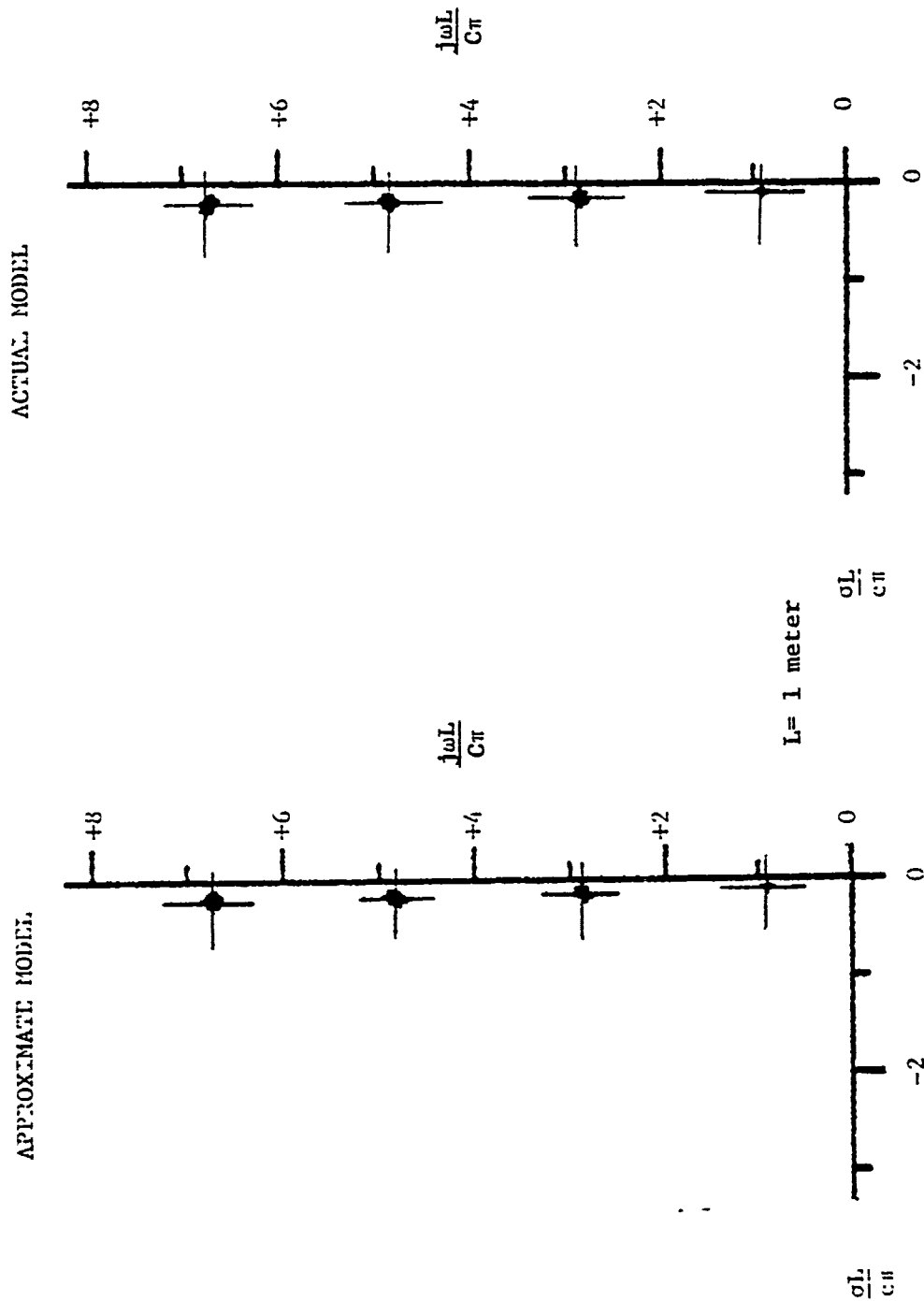waveform is plotted under the noisy waveform for comparison.

Figure 13 Poles for the center-driven TWTD data, SNR = 20 db. The large crosses indicate Tesche's values.

Table 11   Poles for the center-driven TWTD data, SNR = 20 dB.
Results are for the approximate model.

Monte Carlo run: 1

1		2		3	
Real	Imag	Real	Imag	Real	Imag
-.1210	-4.861	-.1342	-7.155	.5749E-01	-6.767
-.1010	.9133	-.9868E-01	-.9369	-.4548E-02	2.899
-.1458	7.516	-.7794E-01	5.217	.2580E-01	9.595
-.1210	4.861	-.1342	7.155	.3627E-01	6.827
-.1634	-2.947	-.1602	2.933	-.8543E-01	-4.707
-.1010	-.9133	-.1602	-2.933	-.1555	4.874
-.1634	2.947	-.9868E-01	.9369	-.4192E-01	-.9497
-.1458	-7.516	-.7794E-01	-5.217	-.5891E-01	.9433

4		5	
Real	Imag	Real	Imag
.8662E-01	-6.593	-.2142	-6.568
.1720	8.959	-.1762	-4.639
-.2584E-01	2.897	-.2142	6.568
-.3866E-01	5.586	-.1762	4.639
-.2593E-01	-2.861	-.7761E-01	.9110
-.2474E-03	-4.842	-.1053	-2.782
-.5955E-01	-.8989	-.7761E-01	-.9110
-.6209E-01	.9237	-.1053	2.782
(non convergent)			

Table 12   Poles for the center-driven TWTD data, SNR = 20 dB.
Results are for the actual model.

Monte Carlo run:

1

Real	Imag
-.2387	-4.953
-.1322	.9218
-.2680	7.441
-.2387	4.953
-.2529	-2.991
-.1322	-.9218
-.2529	2.991
-.2680	-7.441
(non convergent)	

2

Real	Imag
-.2338	-6.908
-.1261	-.9441
-.2784	5.037
-.2338	6.908
-.2380	2.944
-.2380	-2.944
-.1261	.9441
-.2784	-5.037
(non convergent)	

3

Real	Imag
-.3080E-01	-6.768
-.1611	2.889
-.2358	9.027
-.6666E-01	6.835
-.2928	-4.893
-.4115	4.948
-.8578E-01	-.9389
-.1060	.9287
(non convergent)	

4

Real	Imag
-.7754E-01	-6.633
-.3585	-9.651
-.4145E-01	2.860
-.1255	5.696
-.6661E-01	-2.857
-.9278E-01	-4.817
-.7889E-01	-.9011
-.7535E-01	.9164
(non convergent)	

5

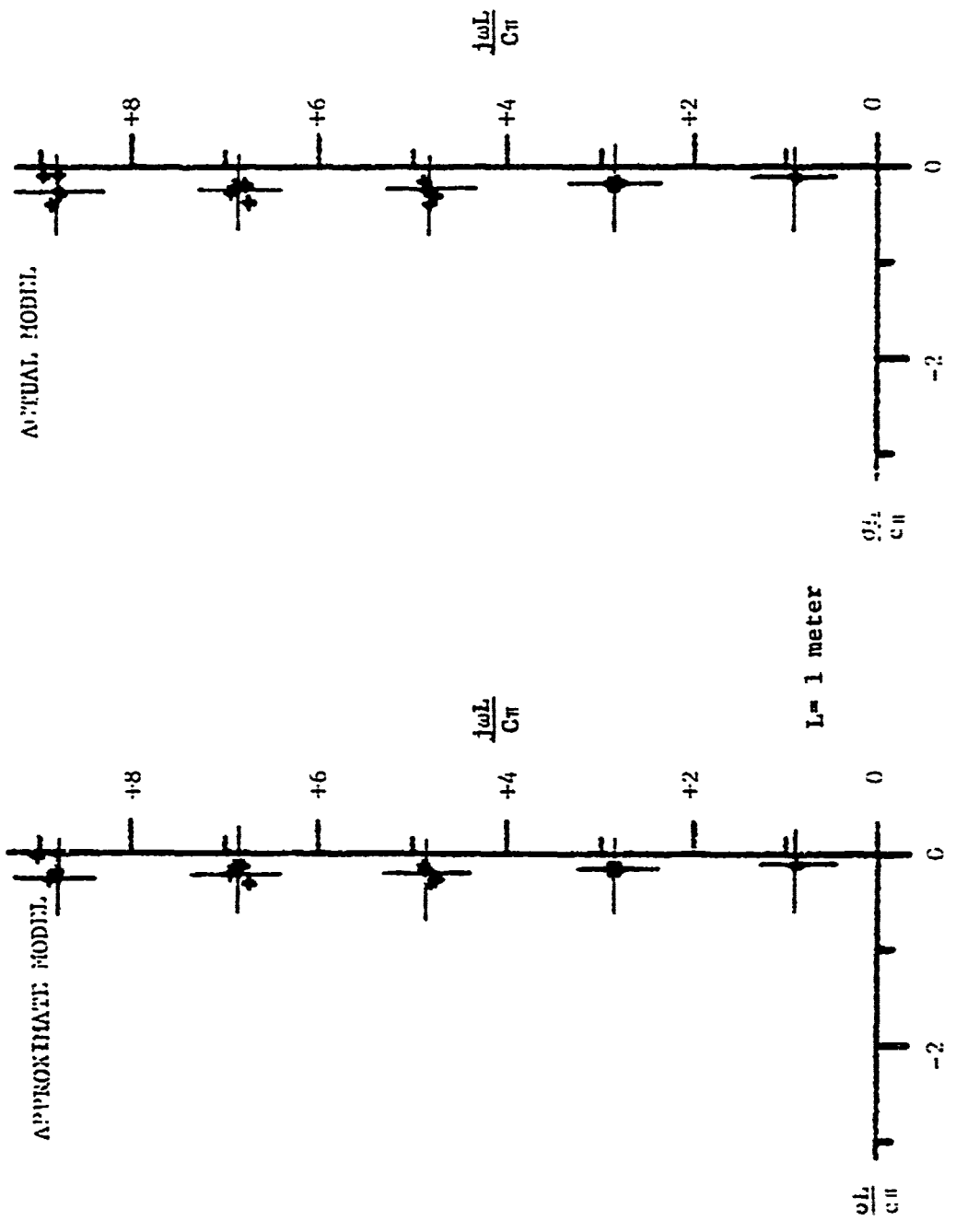| Real	Imag
-.3701	-6.471
-.2955	-4.644
-.3701	6.471
-.2955	4.644
-.8846E-01	.8996
-.1485	-2.766
-.8846E-01	-.8996
-.1485	2.766

Figure 14   Poles for the center-driven TWTD data, SNR = 25 dB.   The large
             crosses indicate Tesche's values.

Table 13   Poles for the center-driven TWTD data, SNR = 25 dB.
Results are for the approximate model.

Monte Carlo run:

1 Real	Imag	2 Real	Imag	3 Real	Imag
-.1475	-6.903	-.3101	-6.736	-.1277	-6.737
-.1475	6.903	-.1861	8.822	.6944	-3.925
-.1185	.9031	-.1861	-8.822	-.1621	4.889
-.2017	8.814	-.2587	4.757	-.4030E-01	9.042
-.1185	-.9031	-.2587	-4.757	-.1918	-4.834
-.1860	-2.874	-.3101	6.736	-.1325	6.806
-.1860	2.874	-.8285E-01	.9080	-.9154E-01	.9176
-.1920	4.839	-.1508	-2.817	-.1465	-2.914
-.1920	-4.839	-.8285E-01	-.9080	-.1490	2.894
-.2017	-8.814	-.1508	2.817	-.8939E-01	-.9262
				(non convergent)	

4 Real	Imag	5 Real	Imag
-.2155	-6.951	-.1414	-6.881
-.2851	8.901	-.1666	2.917
-.1535	2.827	-.1272E-01	-8.808
-.2910	4.818	-.1414	6.881
-.1535	-2.827	-.1175	-4.891
-.2851	-8.901	-.1175	4.891
-.8306E-01	-.8998	-.9697E-01	-.9240
-.2155	6.951	-.1272E-01	8.808
-.2910	-4.818	-.9697E-01	.9240
-.8306E-01	.8998	-.1666	-2.917

Table 14   Poles for the center-driven TWTD data, SNR = 25 dB. Results are for the actual model.

Monte Carlo run:

1		2		3	
Real	Imag	Real	Imag	Real	Imag
-.2006	-6.904	-.3656	-6.745	-.1795	-6.719
-.2006	6.904	-.2445	8.815	.2118	-4.345
-.1195	.9009	-.2445	-8.815	-.2283	4.878
-.2843	8.794	-.2941	4.769	-.8176E-01	8.972
-.1195	-.9009	-.2941	-4.769	-.1876	-5.020
-.1982	-2.864	-.3656	6.745	-.1959	6.774
-.1982	2.864	-.8502E-01	.9049	-.9999E-01	.9139
-.2281	4.833	-.1622	-2.815	-.1369	-2.884
-.2281	-4.833	-.8502E-01	-.9049	-.1717	2.885
-.2843	-8.794	-.1622	2.815	-.9145E-01	-.9236
				(non convergent)	

4		5	
Real	Imag	Real	Imag
-.2727	-6.953	-.1861	-6.872
-.3926	8.884	-.1775	2.913
-.1700	2.819	-.6740E-01	-8.804
-.3850	4.833	-.1861	6.872
-.1700	-2.819	-.1403	-4.885
-.3926	-8.884	-.1403	4.885
-.8443E-01	-.8959	-.9942E-01	-.9230
-.2727	6.953	-.6740E-01	8.804
-.3850	-4.833	-.9942E-01	.9230
-.8443E-01	.8959	-.1775	-2.913

The preprocessing of the waveforms was done primarily to reduce the number of samples that the method is required to process in order to improve efficiency. The preprocessing also reduces the noise level of the waveform although the information content of the waveforms remains the same. The performance of any method should be judged by how well it uses available information instead of by how large a SNR it can tolerate.

Attempts to analyze waveforms consisting of highly damped exponential components, such as the transient responses of a sphere, were not successful. The adaptive method does not converge for such waveforms which display double pole characteristics, that is, waveforms wi h components of the form $t \exp(st)$. Slight modifications to the adaptive method might allow the analysis of such waveforms. The description of these modifications will have to wait until further study is completed in this direction.

Chapter V

CONCLUSIONS AND FUTURE DIRECTIONS

This document has related three identification methods, namely
the pencil-of-function method, Prony's method, and the adaptive
method to the general identification scheme presented in Chapter II.
Each method results, fundamentally, from a certain choice for the fil-
ters in the general identification model. A meaningful way to sum-
marize the relation between the three methods is to plot the transfer
functions of their respective filters as shown in Figure 15. It should
be pointed out that the filters of Prony's method and the pencil-to-
functions method are cascaded, while the filters of the adaptive method
are not. The poles of the discrete filters have been mapped into the
S-plane with the mapping defined by: $z = \exp(sT)$. The filters of
Prony's method treat all frequencies in an equal manner; the filters
of the pencil-of-functions method are preferential to the low fre-
quencies; those of the adaptive method possess passbands which
are adjustable.

The adaptive method is a new method which, in many cases, pro-
vides excellent poles estimates under difficult conditions. The
method is unique in that a solution to a polynomial is not required
to find estimates of the process poles. The method, in effect,
"swallows" the polynomial solver in its own iterative pole-searching
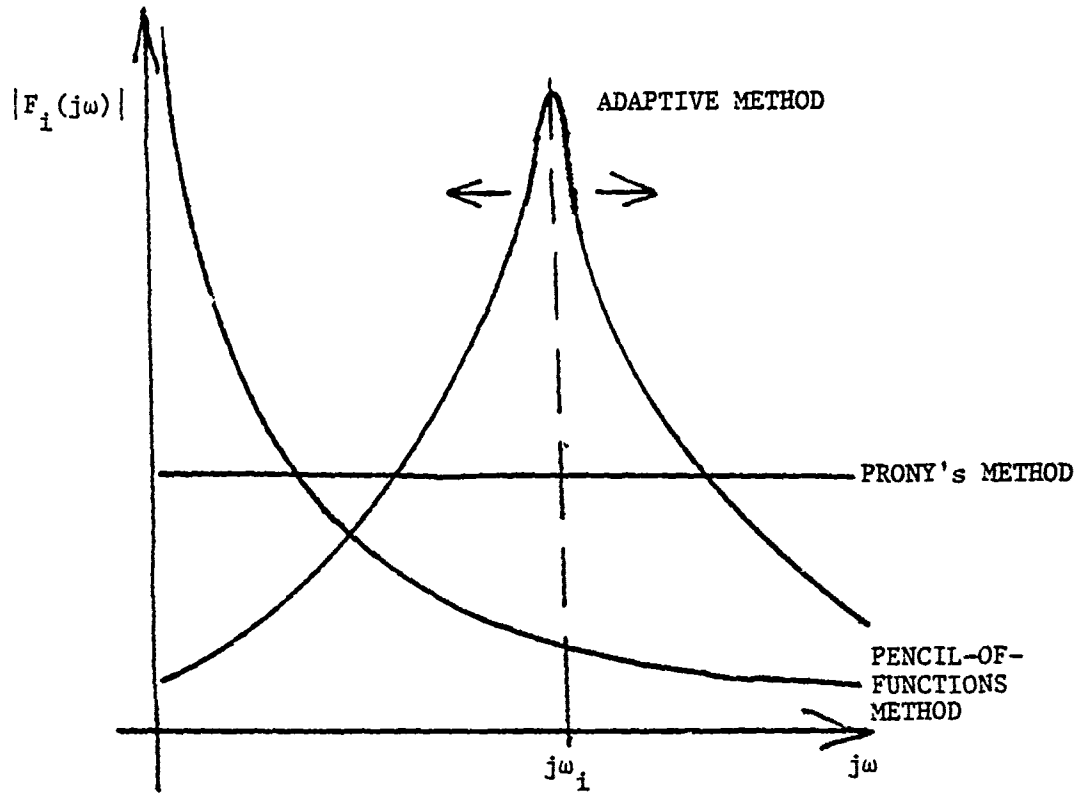
-63-

Figure 15   Illustrative plot of the magnitudes of the transfer
functions of each method as a function of frequency.

scheme. The adaptive method is thought to be closely related to the

method of Steiglitz and McBride [19] since both models filter the in-

put and output records with filters whose poles are the most recent

estimates of the process poles. However, the method of Steiglitz and

McBride does not provide pole estimates but only estimates of the

process transfer function during the course of iteration. The primary

utility of the adaptive method, in the author's opinion, lies in re-

finement of predetermined poles.

The pencil-of-function method was found to be ill-conditioned for

the identification of high order processes. Although the method can

provide superior estimates of low-order processes. It is shown that

use of the $\sqrt{\Delta_{ii}/\Delta_{oo}}$ in place of the α_i was less accurate in general,

than using equation (4) or (6) to estimate the α_i for the approximate

model. Since the parameter values themselves are transplanted into

the actual model, it is not clear if the $\sqrt{\Delta_{ii}/\Delta_{oo}}$ or the α_i more

accurately portray the process after this transplant. But there is no

reason to believe the $\sqrt{\Delta_{ii}/\Delta_{oo}}$ provide a better estimate after the

transplant and every reason to believe that they do not.

Dudley [11] indicated that the noise sensitivity of least-squares

Prony's method was due to parameter bias. In this document, the

parameter bias has been related to the transplanting of parameters

from the approximate model to the true model. Past workers have

applied an ad hoc technique that partially alleviates the noise sen-

sitivity of Prony's method. This technique consists of setting

$M = 2n$ (no redundant data) and setting the model order, n, de-

liberately high to make M large. Since M is the number of samples used in the estimation procedure, a large value of M corresponds to using a lot of data. Hence, this ad hoc technique uses a large amount of data just as least-squares Prony's method does but does not suffer from the parameter bias of the least-squares method. Unbiased parameters result because when $M = 2n$, the least-squares procedure reduces to a curve-fitting procedure which must be unbiased. One side effect of this technique is that extra "curve-fitting poles" which do not correspond to process poles are introduced in the desired exponential representation.

The general identification scheme presented in this work opens up a whole range of possible techniques that can be invented simply by making different choices for the filters within the identification model. One direction in which future research may be fruitful is in inventing schemes, other than least-squares schemes, to combine more data than is necessary to determine the model parameters. Such a scheme could, perhaps, be realized with certain choices for the filters in the identification model.

APPENDIX

Theorem: If G is a singular, complex or real, $N \times N$ dimensional matrix, then $\Delta_{ij}\Delta_{ji} = \Delta_{ii}\Delta_{jj}$ for any i or j, where Δ_{pq} denotes the element of the pth row and the qth column of adj G (that is, the cofactor of g_{pq}.)

Proof: Since G is singular, det G=0. Also, from the identity I det G = G adj G, it follows that G adj G = 0. Each column of adj G then must be a solution of $G\underline{x} = 0$. Since all solutions of $G\underline{x} = 0$ are collinear, it follows that the columns of adj G are also collinear. Hence,

$$\text{adj } G = \begin{bmatrix} x_1 y_1 & x_1 y_2 & \cdots & x_1 y_N \\ x_2 y_1 & x_2 y_2 & \cdots & x_2 y_N \\ \cdot & \cdot & & \cdot \\ \cdot & \cdot & & \cdot \\ \cdot & \cdot & & \cdot \\ x_N y_1 & x_N y_2 & \cdots & x_N y_N \end{bmatrix} = \underline{x}\,\underline{y}^T \qquad (23)$$

where $\underline{x} = [x_1 x_2 \ldots x_N]^T$ is a solution of $G\underline{x}=0$ and $\underline{y} = [y_1 y_2 \ldots y_N]^T$ is the vector required for equality of (23). Then, $\Delta_{ij}\Delta_{ji} = (x_i y_j)(x_j y_i) = (x_i y_i)(x_j y_j) = \Delta_{ii}\Delta_{jj}$.

References

1. P. Eykhoff, "Process parameter and state estimation," *Automatica*, 1968, Vol. 4, pp. 208-234.

2. P. Eykhoff, "Some fundamental aspects of process-parameter estimation," *IEEE Trans. Auto. Control*, October 1963, pp. 347-357.

3. K. J. Astrom and P. Eykhoff, "System Identification - A Survey," *Automatica*, 1971, Vol. 7, pp. 123-162.

4. P. Eykhoff, *System Identification*, Wiley Interscience: New York, 1974.

5. R. Mittra and M. L. Van Blaricum, "A Novel Technique for Extracting the SEM Poles and Residues of System Directly from its Transient Response," 1974 Annual URSI Meeting, University of Colorado, Boulder, Colorado, October 14-17, 1974.

6. C. E. Baum, "On the Singularity Expansion Method for the Solution of Electromagnetic Interaction Problems," *Interaction Note 88*, Air Force Weapons Laboratory, Kirtland AFB, NM, December 11, 1971.

7. C. E. Baum, "The Singularity Expansion Method," Ch. 3 of *Transient Electromagnetic Fields*, L. B. Felsen, ed., Springer-Verlag, Heidelberg, 1976.

8. M. L. Van Blaricum and R. Mittra, "A Technique for Extracting the Poles and Residues of a System Directly from its Transient Response," *IEEE Trans. Antennas Propagat.*, Vol. AP-23, No. 6, Nov. 1975, pp. 777-781.

9. M. L. Van Blaricum and R. Mittra, "Techniques for Extracting the Complex Resonances of a System directly from its Transient Response," Air Force Weapons Laboratory Report No. 76-250, Air Force Weapons Laboratory, Kirtland Air Force Base, NM, April 1977.

10. L. W. Pearson and D. R. Roberson, "The Extraction of the Singularity Expansion Description of a Scatterer from Sampled Transient Surface Current Response," *IEEE Trans. Ant. and Prop.*, AP-28, March 1980, pp. 182-190. See also *Interaction Note 360*, Air Force Weapons Laboratory, Kirtland AFB, NM, October 1978.

11. D. G. Dudley, "Parametric modeling of transient electromagnetic systems," Radio Science, May-June 1979, pp. 387-396. Also appeared in AFWL Mathematics Note 51, Air Force Weapons Laboratory, Kirtland AFB, NM, March 7, 1977.

12. R. E. Kalman, "Design of a Self-Optimizing Control System," Transactions of the ASME, January 1958, pp. 468-478.

13. K. Steiglitz and L. E. McBride, "A technique for the identification of linear systems" (short paper), IEEE Transactions on Automatic Control, AC-10, 1965, pp. 461-464.

14. T. K. Sarkar, J. Nebat, and D. D. Weiner, "Suboptimal system approximation/identification with known error," AFWL Mathematics Note 49, Air Force Weapons Laboratory, Kirtland AFB, NM, September 1977.

15. T. K. Sarkar, V. K. Jain, J. Nebat, and D. D. Weiner, "A comparison of the pencil-of-function method with Prony's method, Wiener Filters and other identification techniques," AFWL Mathematics Note 54, Air Force Weapons Laboratory, Kirtland AFB, NM, December 1977.

16. V. K. Jain and R. D. Gupta, "Identification of linear systems through a Grammian technique," International Journal of Control, Vol. 12, 1970, pp. 421-431.

17. V. K. Jain, "Decoupled method for approximation of signals by exponentials," IEEE Transactions on Systems Science and Cybernetics, July 1970, pp. 244-264.

18. V. K. Jain, "Representation of sequences," IEEE Transactions on Audio and Electroacoustics, Vol. AU-19, September 1971, pp. 208-215.

19. V. K. Jain, "Filter analysis by use of pencil functions: Parts I and II," IEEE Transactions and Circuits and Systems, Vol. CAS-21, No. 5, September 1974.

20. R. N. McDonough and W. H. Huggins, "Best least-squares representation of signals by exponentials," IEEE Transactions on Automatic Control, Vol. AC-13, August 1968, pp. 408-412.

21. L. E. McBride, Jr., H. W. Schaefgen, and K. Steiglitz, "Time-domain approximation by iterative methods," IEEE Transactions Circuit Theory, Vol. CT-13, December 1966, pp. 381-387.

22. P. R. Aigrain and E. M. William, "Synthesis of n-reactants networks for desired transient response, J. Appl. Phys., Vol. 20, June 1949, pp. 597-600.

23. E. G. Evans and Fischl, "Optimal least-squares time-domain synthesis of recursive digital filters, IEEE Trans. Audio Electroacous., Vol. AU-21, February 1973, pp. 61-65.

24. R. Prony, "Essai Experimental et Analytique Sur les Lois de la Dilatabilite de Fluides Elastiques et Sur Celles de la Force Expansive de la Vapeur de L'Alkool, a Differentes Temperatures," J. l'Ecole Polytech (Paris), Vol. 1, No. 2, 1795, pp. 24-76.

25. M. L. Van Blaricum, "A Bibliography of Prony's Method," Effects Technology, Inc., Santa Barbara, CA, 1979.

26. D. L. Lager, H. G. Hudson, A. J. Poggio, E. K. Miller, and F. J. Deadrick, "Prony's Method for Time Domain," Mini-Symposium on Modal Analysis of Experi-ental Data, Albuquerque, NM, March 1977.

27. N. I. Achieser, Theory of Approximation, New York: Ungar, 1956.

28. Forsythe and Moler, Computer Solution of Linear Algebraic Systems, Englewood-Cliffs, New Jersey: Prentice-Hall, 1967.

29. L. W. Pearson and Y. M. Lee, "An Experimental Investigation of the King Surface Current Probing Technique in a Transient Application," University of Kentucky Electromagnetics Research Report. Also submitted to IEEE Trans. Ant. and Prop.

30. M. L. Van Blaricum, "A Numerical Technique for the Time-Dependent Solution of Thin-Wire Structure with Multiple Junctions," Electromagnetics Laboratory Report 73-15, University of Illinois, Urbana, Illinois, December 1973.

31. F. M. Tesche, "Application of the Singularity Expansion Methods to the Analysis of Impedance Loaded Linear Antennas," Sensor and Simulation Note 177, Air Force Weapons Laboratory, Kirtland AFB, NM, May 1973.